Controls on organic carbon enrichment in a Permian periglacial setting (Arckaringa Basin)

Thesis submitted in accordance with the requirements of Macquarie University for a Master of Research Degree in Geology, Department of Earth and Planetary Sciences

Natalie Debenham

23 October 2015

MACQUARIE University

TITLE

Controls on organic carbon enrichment in a Permian periglacial setting (Arckaringa Basin)

ABSTRACT

In the Arckaringa Basin, organic carbon (OC) enrichment within the Permo-Carboniferous Stuart Range Formation occurred within syn-sedimentary fault troughs that were scoured by glaciers. This enrichment was facilitated by sytematic variations in water chemistry within these troughs identifying periods of restriction and open water exchange with the ocean to the south. The U-shaped morphology of some of these troughs apparent in seismic profiles along with the presence of lonestones, dropstones, and feldspathic, angular sediment identifies a cold palaeoclimate depositional setting that is unusual for the organic enrichments of up to 12% total organic carbon (TOC). It is hypothesised that episodic restriction within these fjord-like troughs led to cyclical variations in sulphur concentration within the water column, driving sulfurization reactions that preserved organic matter in discreet laminae. Abundant pyrite (up to 20 wt%) and the distribution of organosulphur compounds with TOC supports this hypothesis. Cyclical oxygenation of bottom waters and alkalinity from OM mineralisation by bacterial sulphate reducers resulted in the formation of manganese carbonate (kutnohorite) during periods of ventilation. Organic-lean sediments in the adjacent lacustrine Cooper Basin that lacked a source of marine sulphur do not show vulcanization nor preservation of labile organic matter.

KEYWORDS

Arckaringa Basin, organic carbon, preservation, sulfurization, cold-climate, source rock

STATEMENT OF ORIGINALITY

The work presented here is the result of my own original research, except where acknowledged in the text. It has not been submitted to any other university or institution.

N. Debenham

TABLE OF CONTENTS

Title i
Abstract i
Keywords i
Statement of Originality i
List of Figures 2
List of Tables 2
Introduction 3
Geological Setting 5
Methods 10
Sample Collection 10
Basin Geology Methods 10
Geochemical Analyses 10
Mineralogical Analyses 11
Petrographical and Petrophysical Analyses 11
Seismic Profile Analyses 11
Organic Geochemistry Methods 13
Results and Observations 14
Basin Morphology 15
Sediments of the Stuart Range Formation from Arck 1 core 20
Proglacial Facies 20
Pelagic Facies 24
Cyclic Varve Unit (sub-facies 2a) 31
Massive Black Shale (sub-facies 2b) 32
Lensed Mudstone (sub-facies 2c) 32
Bioturbated Facies 33
Mass flow facies 33
Source Rock Characterisation 34
Organic Geochemistry 37
Discussion 40
Conclusions 48
Acknowledgments 49
References 49
Appendix A: Organic geochemistry data 55
Appendix B: XRD data 55
Appendix C: Sample data 57

LIST OF FIGURES

Figure 1: Location map of the Arckaringa Basin in South Australia, Australia 5
Figure 2: Schematic cross section through the Arckaringa Basin 6
Figure 3: Late Carboniferous to early Permian palaeogeographic reconstruction, Arckaringa Basin 9
Figure 4: Surface contamination and drilling fluid residue removed from drill core surfaces 13
Figure 5: Base Permian depth structure map of the Arckaringa Basin in South Australia 14
Figure 6: Orientation of seismic lines 86AK-3B, 86AK-8 and 86AK-7 from 1986 and GOMA seismic line 08GA-OM1 from 2008 15
Figure 7: Interpretation of seismic lines 86AK-3B, 86AK-8, and 86AK-7 from 1986, together with 2008 GOMA seismic line 08GA-OM1 16
Figure 8: Interpretation of 2008 GOMA seismic line 08GA-OM1 18
Figure 9: Interpretation of 1986 seismic line 86AK-3B of the Wallira Trough 19
Figure 10: Interpretation of seismic lines 84-XER_mig_08SX (north–south) and 84-XES (west–east) 19
Figure 11: Scanning electron microscope photomicrographs of the compositionally immature nature of the detrital mineral component within the Stuart Range Formation and its relationship to organic matter 21
Figure 12: Core log of Arck 1 22
Figure 13: Representative images and characteristic features of the four facies 23
Figure 14: Representative images and characteristic features of the three Pelagic Facies sub-facies 25
Figure 15: Scanning electron microscope and integrated energy dispersive X-ray spectroscopy photomicrographs of polished blocks taken from the Pelagic Facies 26
Figure 16: Clay mineral fraction X-ray diffractogram of Arck 1 Pelagic Facies 27
Figure 17: Reflected light and ultra-violet photomicrographs showing organic components 28
Figure 18: Quantitative Evaluation of Minerals by Scanning electron microscopy mineral maps 30
Figure 19: Scanning electron microscope photomicrograph of the Massive Black Shale 31
Figure 20: The types of hydrocarbons and the maturity of a selection of Arck 1, Cootanoorina 1, and Lambina 1 core samples, based on source rock analysis 36
Figure 21: Representative source rock potential pyrograms based on source rock analysis 37
Figure 22: Organosulphur compounds with percentage total organic carbon 38
Figure 23: Ternary diagram of C_{27}, C_{28}, and C_{29} ααα R sterane proportions (%) 39
Figure 24: A plot of C_{24} tetracyclic terpanes/(C_{24} tetracyclic terpanes+C_{23} tricyclic terpanes) against C_{19} tricyclic terpanes/(C_{19} tricyclic terpanes+ C_{23} tricyclic terpanes) 40
Figure 25: Schematic diagram illustrating changes in bottom water redox conditions 47

LIST OF TABLES

Table 1: Stratigraphic descriptions of the Arckaringa Basin formations and Cootanoorina Formation 7
Table 2: Summary drill core and sampling information for Arck 1, Cootanoorina 1, and Lambina 1 10
Table 3: Classification table for the identification of organic macerals 12
Table 4: Method 2 settings of the Dionex 300 Accelerated Solvent Extractor 14
Table 5: Reflector characteristics used for the interpretation of each formation in seismic profiles 17
Table 6: Typical mineralogy of the four facies identified within the lower Stuart Range Formation. 24

INTRODUCTION

Organic carbon (OC) rich rocks are globally important long-term sinks of carbon. They host significant economic mineral deposits (Speczik 1995) and serve as source rocks for both conventional and unconventional hydrocarbon systems (Aplin and Macquaker 2011; Macquaker *et al.* 2014). Not withstanding their broad environmental and economic relevance, the origins and properties of organic-rich mudstones remarkably remain poorly understood. This is largely because of the fine grain size of these deposits. Their often homogeneous appearance at hand specimen scale has led to the perception of an undifferentiated, mineralogically homogenous rock deposited by pelagic settling in low-energy, low-oxygen environments (Macquaker *et al.* 2007; Aplin and Macquaker 2011). However, recent studies emphasing careful microscopic analysis, together with new technological developments allowing imaging of shale grains at nanometre scales, is starting to draw a more complex picture (Schieber 1999; Macquaker *et al.* 2010; Schieber *et al.* 2010; Alexandre *et al.* 2011). These studies reveal an unexpected degree of mineralogic, diagenetic and organic heterogeneity reflecting complex depositional and diagenetic processes.

OC-rich intervals of the Permo-Carboniferous Arckaringa Basin, South Australia, have generated intense interest in the last decade. Recent hydrocarbon exploration has identified excellent resource play potential, with organic and mineralogic properties and interval thicknesses that compare favourably to prolific USA unconventional plays (Linc Energy Ltd 2013), and independent prospective resource estimates of 103 to 233 billion barrels of oil equivalent (Linc Energy Ltd, 2013). The intervals in question are typically fine-grained siltstones with up to 11% TOC and hydrogen indices of up to 300 mg HC/g TOC, demonstrating potential for a significant hydrocarbon charge (Hunt 1996). However, maturity analysis suggest that the source intervals are presently at the threshold of oil generation, so that there is a significant risk that the thermal maturity of the source interval is not sufficient to have generated hydrocarbon across the basin. Sediments are of increasing thermal maturity in the deeper southern part of the basin, providing a focus for future exploration (Hibburt 1984; Neumann et al. 2010; Menpes 2012).

The remarkable OC enrichment of the Permo-Carboniferous sediments in the Arckaringa Basin is also interesting because these were deposited under conditions very different from those typical of the vast majority of organic carbon rich sediments in the geologic record. The geologic record identifies a strong bias toward accumulations of OC rich shale during greenhouse periods (Klemme and Ulmishek 1991; Weissert and Mohr 1996). By contrast, the Arckaringa Basin

sediments were deposited under restricted marine conditions during the waning stages of glaciation (Wopfner 1970; Jones 1987; Alexander et al. 1998; Veevers 2006). Little is known about the preservation mechanisms of organic carbon responsible for the significant OC enrichment evident within these rocks. Predictive models for source rock prospecting in icehouse periods are also poorly developed. As the search for hydrocarbons becomes more intense, more sophisticated understanding of source rock controls are needed to exploit more diverse hydrocarbon plays, like that potentially offered in the Arckaringa Basin. Thus, it is timely to review the geological development and mechanisms of OC enrichment within the Arckaringa Basin in the light of recent data acquired from seismic imagery and geochemical studies conducted on core from recently drilled exploration.

This thesis shows, from whole core to micron scale, the distribution and variation of OC and mineral phases in Permo-Carboniferous succession of the Arckaringa Basin in order to identify the mechanisms responsible for one of Australia's most organic rich source rocks. This study provides a synthesis of the geological development of the hydrocarbon system and formation of basin morphology. More specifically, the role of restriction and anoxia associated with marine sill development in a fjord is determined. Results from this thesis suggest that marine restriction of the basin troughs led to periods of hydrogen sulphide build up, promoting sulfurization reactions to preserve OC through the incorporation of inorganic S into lipids and carbohydrates to form organosulphur compounds during early diagenesis. Preservation efficiency is expressed within sub-millimetre scale, compositionally distinct organic-rich and organic-lean laminations.

GEOLOGICAL SETTING

The Arckaringa Basin is a Permo-Carboniferous intracratonic basin that covers an area of approximately 100,000 square kilometres in central northern South Australia (Figure 1; Wopfner 1970; Wohling et al. 2013). Two main depocentres, the broad Boorthanna Trough in the east and the narrow Southern Arckaringa Troughs (Wallira, Phenrhyn, Phillipson, and West) in the south, are situated around a basement high associated with the Mount Woods Inlier. The Permo-Carboniferous succession of the Arckaringa Basin comprises three formations defined by drill cores, outcrop mapping, and geophysical exploration (Ludbrook 1967; Townsend and Ludbrook 1975; Wopfner 1980). These formations, in ascending stratigraphic order, are the Boorthanna, Stuart Range, and Mount Toondina Formations (Figure 2; Table 1). These sediments were deposited under restricted marine conditions during the waning stages of glaciation in the Pennsylvanian to early Permian (Figure 3; Wopfner 1970; Alexander *et al.* 1998).

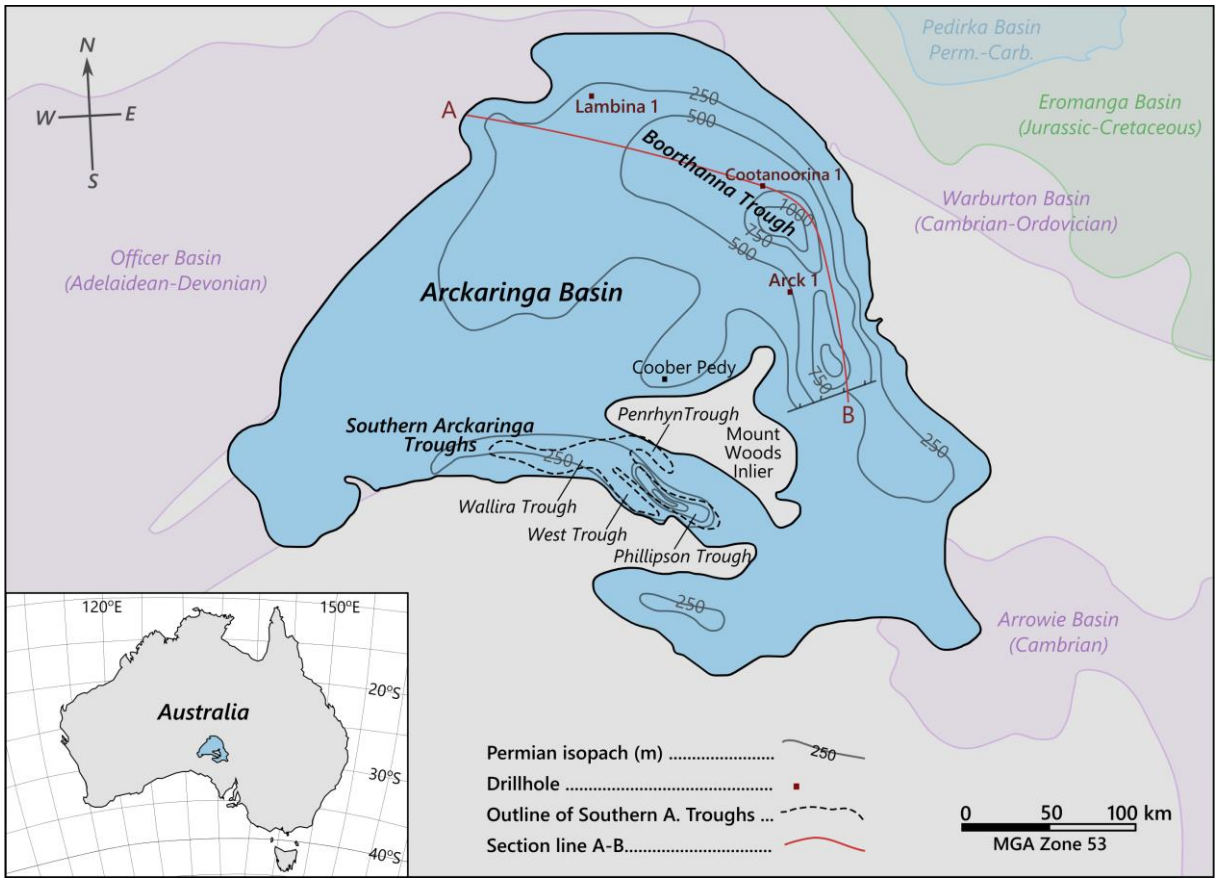

Figure 1: Location map of the Arckaringa Basin in South Australia, Australia (inset) and the position of the basin relative to other basins. The purple Officer, Arrowie, and Warburton Basins are stratigraphically older than the Arckaringa Basin, the blue Pedirka Basin is of similar age, and the green Eromanga Basin is stratigraphically younger. The Boorthanna Trough and Southern Arckaringa Trough are shown. The locations of Arck 1 and Cootanoorina 1 (both within the Boorthanna Trough) and Lambina 1 are also shown, intersected by section line A–B. Permian

isopach lines illustrate the thickness of the subsurface Permian sediments across the basin. Modified after Hibburt (1995) and Menpes (2012).

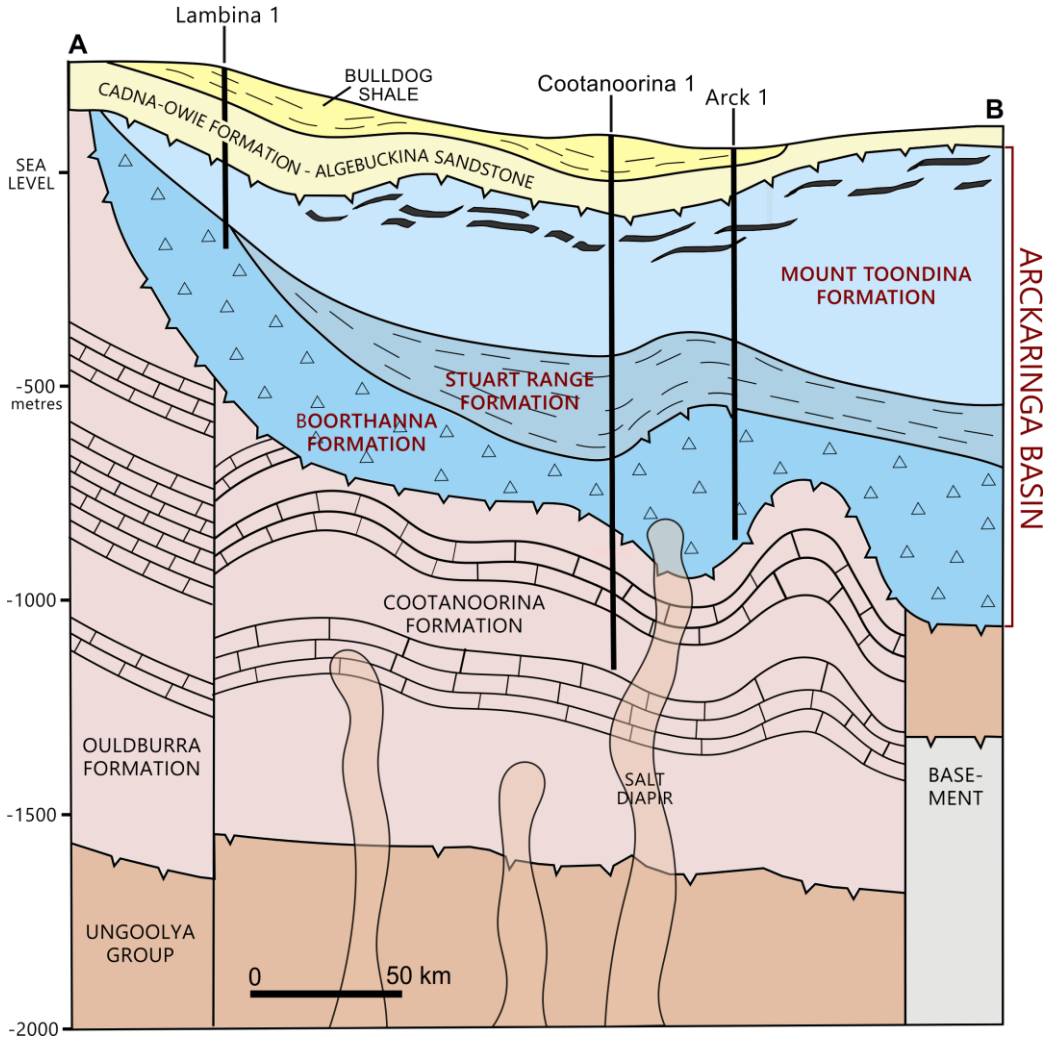

Figure 2: Schematic cross section through the Arckaringa Basin along section line A–B, showing the geometry of the Boorthanna Trough and the formations intersected by Arck 1, Cootanoorina 1, and Lambina 1. The Cootanoorina Formation unconformably underlies the Arckaringa Basin, and within the Arckaringa Basin it is restricted to the Boorthanna Trough. Modified after Hibburt (1995) and Harvey and Hibburt (1999).

Table 1: Stratigraphic descriptions of the Arckaringa Basin formations and underlying Cootanoorina Formation, including age based on palynology and interpreted sedimentary environment of deposition.

Unit	Age based on palynology (Price *et al.* 1985; Wohling *et al.* 2013)	Description	Interpreted sedimentary environment
Mount Toondina Formation	295.0 to 290.1 Ma (Sakmarian), or palynostratigraphic zone PP2	The Mount Toondina Formation overlies the Stuart Range Formation with a conformable to disconformable relationship; however the formation may also unconformably overlie the Stuart Range Formation and the Boorthanna Formation in some areas within the Boorthanna Trough (Hibburt 1984). The Mount Toondina Formation is prevalent across much of the basin, with the thickest intersection of 598 metres in the Boorthanna 1 well. Two units can be identified within the formation; The lower unit consists of interbedded siltstones and clays with minor fine sands, and contains minimal carbonaceous material and is absent of coals. The upper unit is comprised of interbedded siltstones, shales and coal seams up to 10 m thick as well as minor sands, and contains an increased abundance of carbonaceous material.	The formation comprises an overall coarsening upward succession that is capped by coals, consistent with the prograding deltaic to fluvial-lacustrine deposition with intermittent coal swamp development suggested by Menpes (2012), derived from interpretations made by Wopfner (1970) and Townsend and Ludbrook (1975) and geophysical observations from recent drilling activity.
Stuart Range Formation	The lower Stuart Range Fm. has been assigned to zone PP1 (Asselian) and the upper Fm. has been assigned to zone PP2 (Sakmarian), suggesting 298.9 to 290.1 Ma	The Stuart Range Formation conformably overlies the Boorthanna Formation in most areas throughout the basin, although seismic sections indicate an unconformable boundary within the Boorthanna Trough (Hibburt 1984). The formation is widely distributed and encountered in most wells, and has a maximum thickness of 491 metres that was intersected by the Lake Phillipson Bore (Ludbrook 1967; Townsend and Ludbrook 1975). It comprises homogenous shale with occasional thinly laminated siltstone and minor sandstone, and can be micromicaceous, calcareous and pyritic (Hibburt 1984). The sediments were deposited during a marine transgressive phase (Jones 1987), and sequence stratigraphic studies by Menpes (2012) indicate that the maximum flooding surface can be considered as a reasonable marker for the top of the Stuart Range Formation.	Alternating restricted marine and lacustrine depositional conditions are suggested in a number of wells across the basin (Hibburt 1995) by changes in lithology and microfauna assemblages (Harris and McGowran 1968; Hibburt 1984; Hawkes 2014).
Boorthanna Formation	298.9 to 295 Ma (Asselian), or palynostratigraphic zone PP1	The Boorthanna Formation was defined using the Boorthanna 1 well (Townsend and Ludbrook 1975), which provides the representative 419.1 metres thick subsurface type section of the formation. Two units can be identified within the formation which grade from a glaciogene sequence to a marine facies stratigraphically higher. The lower unit appears to be restricted to the deeper parts of the basin, such as	The lower unit of the Boorthanna Formation represents subaqueous glacial debris that may have been transported by mudflows (Hibburt 1995). Many studies suggest the glaciogene

		within the Southern Arckaringa Troughs and the southern half of the Boorthanna Trough. It consists of a glaciogene diamictite of sandy clays and pebble to boulder clays with occasional carbonate intercalations (Wohling *et al.* 2013), and in some wells conglomerates from the local erosion of basement highs have been identified (Ludbrook 1967; Townsend and Ludbrook 1975; Moore 1982). The upper unit is more ubiquitous and is comprised of rhythmically bedded marine clastics with grain sizes that range from silt to boulders. Medium to coarse grained sandstone dominates the unit, often grading to conglomerates composed of basement rock lithologies and occasionally grading into siltstones (Hibburt 1984; Hibburt 1995). Kellett *et al.* (1999) described the Boorthanna Formation sediments as mostly weakly indurated with local calcareous, ferruginous and pyrite cementation.	sediments were transported and deposited by rivers, mudflows and turbidity currents under fluvial and marine conditions (Wopfner 1970; Townsend and Ludbrook 1975; Hibburt 1995).
Cootanoorina Formation	Early Palaeozoic	The Cootanoorina Formation that unconformably underlies the Permo-Carboniferous succession within the Boorthanna Trough comprises a shallow marine siliciclastic to dolomitic and anhydritic sequence and is laterally equivalent to the Ouldburra Formation of the Officer Basin (Jones 1988; Hibburt 1995). The anhydrite shows evidence of significant post-depositional mobilisation (Moore 1982) which could potentially be a result of the Mount Toondina diapiric structure (Allchurch *et al.* 1973; Jones 1988). Gently undulating Neoproterozoic sediments of the Adelaide Rift complex underlie the Cootanoorina Formation. The formation can range up to 1000 metres thick toward the centre of the Boorthanna Trough.	Interpreted to have been deposited as a predominately shallow marine and evaporitic tidal flat (Moore 1982).

The Cootanoorina Formation is a microcrystalline, siliciclastic to dolomitic and anhydritic sequence that is interpreted to have been an evaporitic tidal flat or sabkha (Table 1; Jones 1988; Hibburt 1995). The evaporitic tidal flat interpretation and the lateral extent of the early Cambrian Cootanoorina Formation suggests that basin topography must have formed after deposition. During the late Cambrian a series of tectonic events resulted in the formation of zones of crustal weakness (Wohling *et al.* 2013). The initiation of north-west trending lineaments and subsequent down-faulting along these zones of crustal weakness are recorded by compressional structures during the Devonian, perhaps the result of deformation within the Alice Springs Orogeny (Wopfner 1970; Jensen-Schmidt *et al.* 2006). Apatite Fission Track and Zircon-Helium age populations record a period of Carboniferous exhumation and erosion throughout South Australia and the Peake and Denison Ranges (adjacent to the Arckaringa Basin), interpreted to be a result of deformation within the Alice Springs Orogeny (Gleadow *et al.* 2002; Kohn *et al.* 2002; Hall 2014; Weisheit *et al.* 2014). Carboniferous deformation from the New England Orogen, in eastern Australia, may have also coalesced with the deformation within the Alice Springs Orogeny to enhance this exhumation and erosion within South Australia and influence basin topography (Wopfner 1980; Glen 2005).

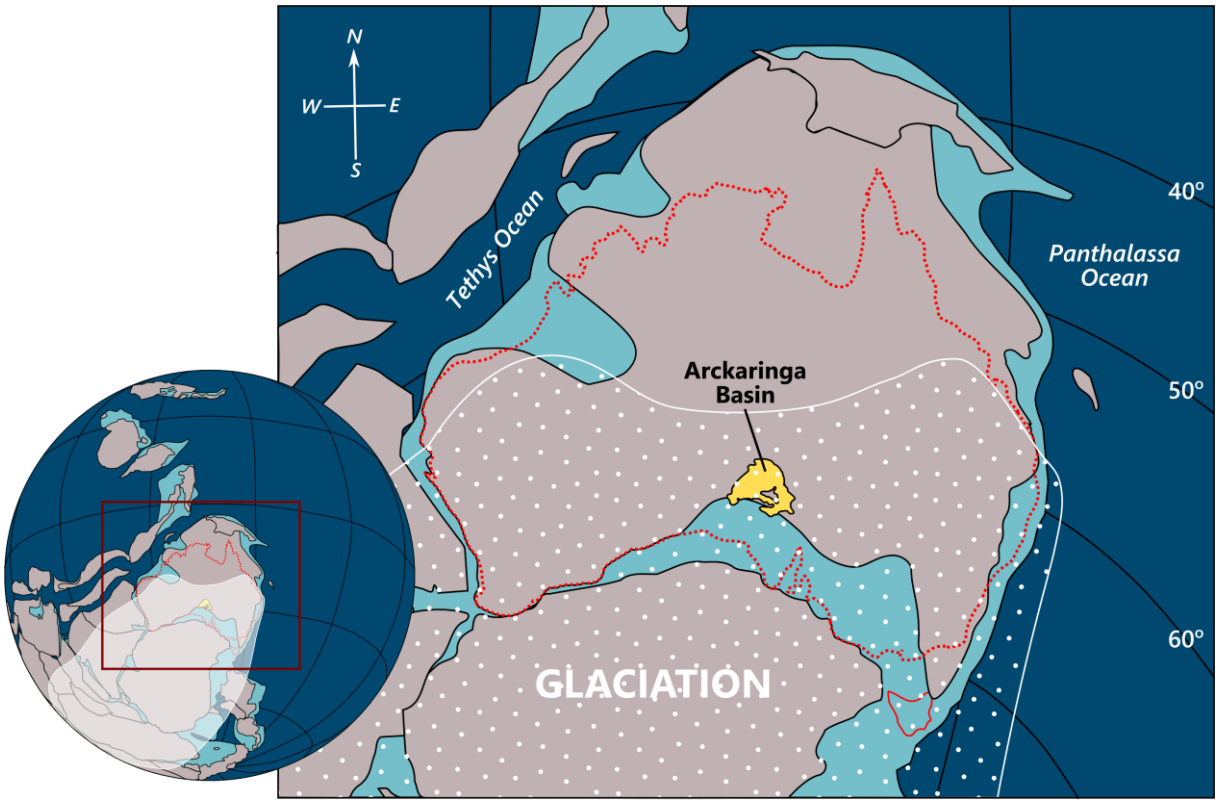

Figure 3: Late Carboniferous to early Permian palaeogeographic reconstruction of the Arckaringa Basin (yellow). The approximate extent of exposed continental crust (brown), glaciation (white dots), the continental shelf (light blue) have been illustrated. The modern coastline of Ausralia is outlined in red. Modified after Li and Powell (2001) and Veevers (2006).

METHODS

Sample Collection

Core samples were collected from Arck 1, Cootanoorina 1, and Lambina 1 at the DMITRE drill core library, South Australia. Arck 1 and Cootanoorina 1 were drilled within the Boorthanna Trough (Figure 1) and reach similar depths (Table 2), although the Permo-Carboniferous succession in Arck 1 is deeper. Lambina 1 was drilled near the northern boundary of the Arckaringa Basin. The thicknesses of core studied were 118 m (Arck 1), 75 m (Cootanoorina 1) with 168m of cuttings inspected from Cootanoorina 1, and 63 m (Lambina 1). Samples were selected for geochemical, mineralogical, and petrographical analyses to illustrate the geochemical and sedimentological variability across the Permo-Carboniferous formations and the underlying Cootanoorina Formation.

Table 2: Summary of the drill core and sampling information for Arck 1, Cootanoorina 1, and Lambina 1, acquired from the Arck 1, Cootanoorina 1 and Lambina 1 well completion reports.

	Arck 1	Cootanoorina 1	Lambina 1
Max. drilled date	17-08-2011	15-06-1967	31-03-1970
Operator	Linc Energy Ltd.	S.A. Dept. Mines and Energy	S.A. Dept. Mines and Energy
Exploration tenement	PEL 122	–	OEL 20
Latitude	28° 30' 12.48" S	28° 00.5' 23.218" S	27° 30' 54.777" S
Longitude	135° 29' 10.37" E	135° 19' 59.632" E	134° 17' 12.718" E
Formations intersected	Mount Toondina Fm. to upper Boorthanna Fm.	Mount Toondina Fm. to Cootanoorina Fm.	Mount Toondina and Boorthanna Fm.
Core depth sampled	876.13–994.10 m	380.09–948.06 m	440.13m, 441.96m
Cutting depth sampled	–	701.04–871.73 m	377.95m, 411.48m, 435.86m
Inspection number(s)	4194, 4337, 4445	4278	–

Basin Geology Methods

GEOCHEMICAL ANALYSES

A total of 271 sub-samples (comprising 186 core samples from Arck 1, 25 core and 55 cutting samples from Cootanoorina 1, and 5 core samples from Lambina 1) were milled to a fine powder for a number of geochemical and mineralogical analyses. Total carbon (TC) content was measured for all samples using a PerkinElmer® 2400 Series II CHNS/O Elemental Analyser. Inorganic carbon (IC) content was determined using the modified pressure-calcimeter method of Sherrod *et al.* (2002). Total organic carbon (TOC) content was subsequently calculated by batch subtraction, i.e. TOC (%) = TC (%) – IC (%). Source rock properties such as the proportion of free

hydrocarbons (S_1) and the proportion of hydrocarbons with generative potential (S_2), were determined by pyrolysis-induced maturation of organic carbon in a Weatherford® Laboratories Source Rock Analyser (SRA) TPH utilising the Rock-Eval pyrolysis method of Espitalié *et al.* (1977). Also obtained from the SRA was thermal maturity, which was estimated using Tmax following Jarvie *et al.* (2001).

MINERALOGICAL ANALYSES

The bulk mineralogy of a selection of powdered samples taken from Arck 1 was ascertained by a Bruker D8 ADVANCE Powder X-ray Diffraction (XRD) with a Cu-radiation source, using Bruker DIFFRAC.EVA software and Crystallography Open Database reference patterns for identifying mineral phases. Mineralogy was also examined by scanning electron microscope (SEM) analyses, using energy dispersive x-ray spectroscopy (EDS) systems (detailed further below). Quantitative Evaluation of Minerals by Scanning electron microscopy (QUEMSCAN® by FEI Company) mineral mapping, using energy-dispersive X-ray spectroscopy (EDS) for data acquisition, was undertaken on two representative samples.

PETROGRAPHICAL AND PETROPHYSICAL ANALYSES

Core samples were cut perpendicular to the bedding plane and the blocks were milled and polished using a Fischione 1010 Argon Ion Mill or a Hitachi IM4000 Ion Milling systems. Cutting samples were mounted in cold setting epoxy (araldite and hardener), ground and polished by hand. Reflected white light and fluorescence (UV and blue light) microscopy was performed using a polarised microscope for organic petrography analyses in order to identify the organic matter present. Sample preparation and analyses were conducted following the methodology and identification standards of Taylor *et al.* (1998) and Suárez-Ruiz *et al.* (2012) based on the ICCP (International Committee for Coal Petrology) System of 1994 (Table 3). The same samples were subsequently carbon coated and imaged by SEM (FEI Quanta 450 SEM and Joel Neoscope JCM 6000 SEM in back scattered electron mode) to identify variations in composition, diagenetic alteration, and textural relationships.

SEISMIC PROFILE ANALYSES

A selection of seismic profiles completed between 1980 and 1989 were used for analysis of the Southern Arckaringa Troughs. Seismic profiles collected since 2010 were used for analysis of the Boorthanna Trough. Seismic line 08GA-OM1, from the 2008 Gawler Craton-Officer Basin-

Musgrave Province-Amadeus Basin (GOMA) seismic survey, transects the Arckaringa Basin along the Adelaide to Alice Springs railway line, and was also investigated. A recent paper by Menpes *et al.* (2010b) with results published on the GOMA seismic survey will form the basis for interpretations.

Table 3: Classification table for the identification of macerals used during organic petrographic analysis, compiled after Taylor *et al.* (1998) and Suárez-Ruiz *et al.* (2012).

Maceral Gp.	Maceral sub-group	Macerals	Identification	
Vitrinite	**Telovitrinite**: Intact cell structures	Telinite	Distinct walls in large pieces of woody tissue. Shows cell cavities.	Medium reflectance Higher plant terrestrial origin
		Collotelinite	Homogenous and structureless gelified remains of plant tissue.	
	Detrovitrinite: Detrital	Detrovitrinite	Fragmented vitrinite often associated with inclusions/debris.	
		Collodetrinite	Mottled, dark bands of detrital material that bind other macerals.	
	Gelovitrinite: Dominated by colloidal gelinite material	Gelinite	Formless, structureless gels which fill formerly empty spaces.	
		Corpogelinite	Discrete and homogenous, often fills cell lumens. Can be isolated or in situ.	
Inertinite	**Telo-inertinite**: Intact cell structure	Fusinite	Empty or mineral-filled, well preserved cellular structure. Oxidised ∴ bright.	High reflect. Terrestrial origin
		Semifusinite	Squashed, broken fusinite. Cannot see distinct cell walls or structure.	
		Funginite and secretinite.	Represents fusinised resin bodies, round or oval form, fungi/fungal spores.	
	Detro-inertinite: Detrital	Inertodetrinite	Small, discrete fragments of varying sizes, >2 µm in diameter.	
		Micrinite	Non-angular particles <10 µm in diameter.	
	Gelo-inertinite: Non-structured	Macrinite	Structureless and inert material, occurs as ground mass or <10 µm bodies.	
Liptinite	**Primary liptinite**: H-rich, distinct structures	Sporinite	Spores, defined by thick, distinct walls. Can occur as sporangium.	Low reflect. High fluores-cence Marine and terrestrial origin
		Resinite	Often 'sausage' shaped with a homogenous texture.	
		Cutinite	Upper smooth surface and lower 'saw-tooth' from cuticles.	
		Alginite (also Telginite)	'Cauliflower' appearance. Can occur as algal colonies.	
		Lamalginite	Long and finely banded, thin-walled lamellar alginite.	
		Suberinite	Cork. Lacy/wavy continuous form, often in-filled with corpogelinite or huminite.	
		Liptodetrinite	Small, finely detrital particles that cannot be identified as another.	
		Bituminite	–	
	Secondary liptinite: Break down of	Exsudatinite		

liptinite

Organic Geochemistry Methods

Whole rock samples (Appendix A) were submerged into a solvent mixture composed of dichloromethane (DCM) and methanol (MeOH) (9:1, v/v) and ultrasonicated to eliminate surface contamination and drilling fluid residue. If drill core surfaces were present, these surfaces were cut and kept as a sub-samples in order to compare the potential effects of contamination (Figure 4). Samples were crushed, then extracted twice using a Dionex 300 Accelerated Solvent Extractor (ASE) following Method 2 (Table 4). Elemental sulphur was removed from the resulting extractable organic matter (EOM) using activated copper in order to protect laboratory instrumentation and facilitate peak identification. The EOM was quantified by transferring a 1 ml aliquot from 10 ml of EOM into a pre-weighed vial. The solvent was evaporated from the aliquot by blowing a gentle stream of dry nitrogen over the top of the vial. Once dried, the stable weight of the aliquot was measured.

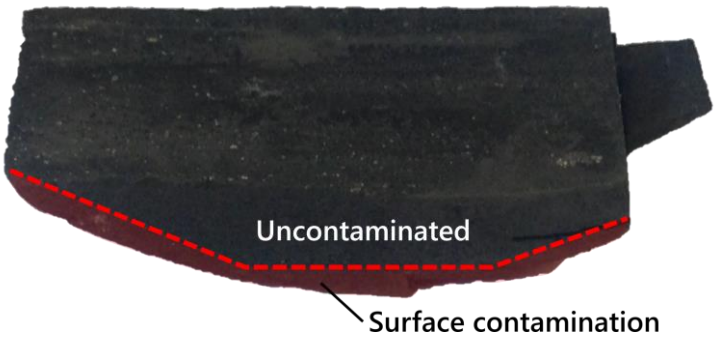

Figure 4: Surface contamination and drilling fluid residue removed from drill core surfaces and set aside for comparative geochemical analysis with uncontaminated rock. Sample 2053188 is shown here.

Following the guidelines of Bastow *et al.* (2007), column fractionation of the EOM was performed to separate the total hydrocarbons from the polar compounds. Modifications to these guidelines included the use of different solvents, for instance, first a standard silica column was made uniform by pouring three beds of 3.5 mL *n*-hexane/DCM (4:1 v/v) through the silica. The total hydrocarbons were separated by eluting with *n*-hexane/DCM (4:1 v/v, 3 mL) and the polar compounds were collected by eluting with methanol/DCM (1:1 v/v, 3 mL). The total hydrocarbons were further fractionated to separate the aliphatic hydrocarbons from the aromatic hydrocarbons. Another standard column was prepared and made uniform using hexane/DCM (4:1 v/v, 3.5 mL). The aliphatic hydrocarbons were collected by eluting with *n*-hexane (2.6 mL), then the aromatic

hydrocarbons were collected by eluting with *n*-hexane/DCM (4:1 v/v, 3.5 mL). The aliphatic and aromatic hydrocarbons were subsequently analysed by gas chromatography-mass spectrometry (GC-MS) on a Leco Pegasus Gas Chromatograph interfaced to a Time-of-Flight Mass Spectrometer run in 1D mode. Identifications of the resultant peaks in mass chromatograms were based on relative retention times and published mass spectra.

Table 4: Method 2 settings of the Dionex 300 Accelerated Solvent Extractor

Mode	Setting	Mode	Setting
Preheat (minutes)	5	Pressure (Psi)	1500
Heat (minutes)	5	Temperature (°C)	100
Static (minutes)	5	Solvent A	90% DCM ($MeCl_2$)
Flush (% volume)	100	Solvent B	10% Methanol (MeOH)
Purge (seconds)	120	Solvent C	–
Cycles	3	Solvent D	–

RESULTS AND OBSERVATIONS

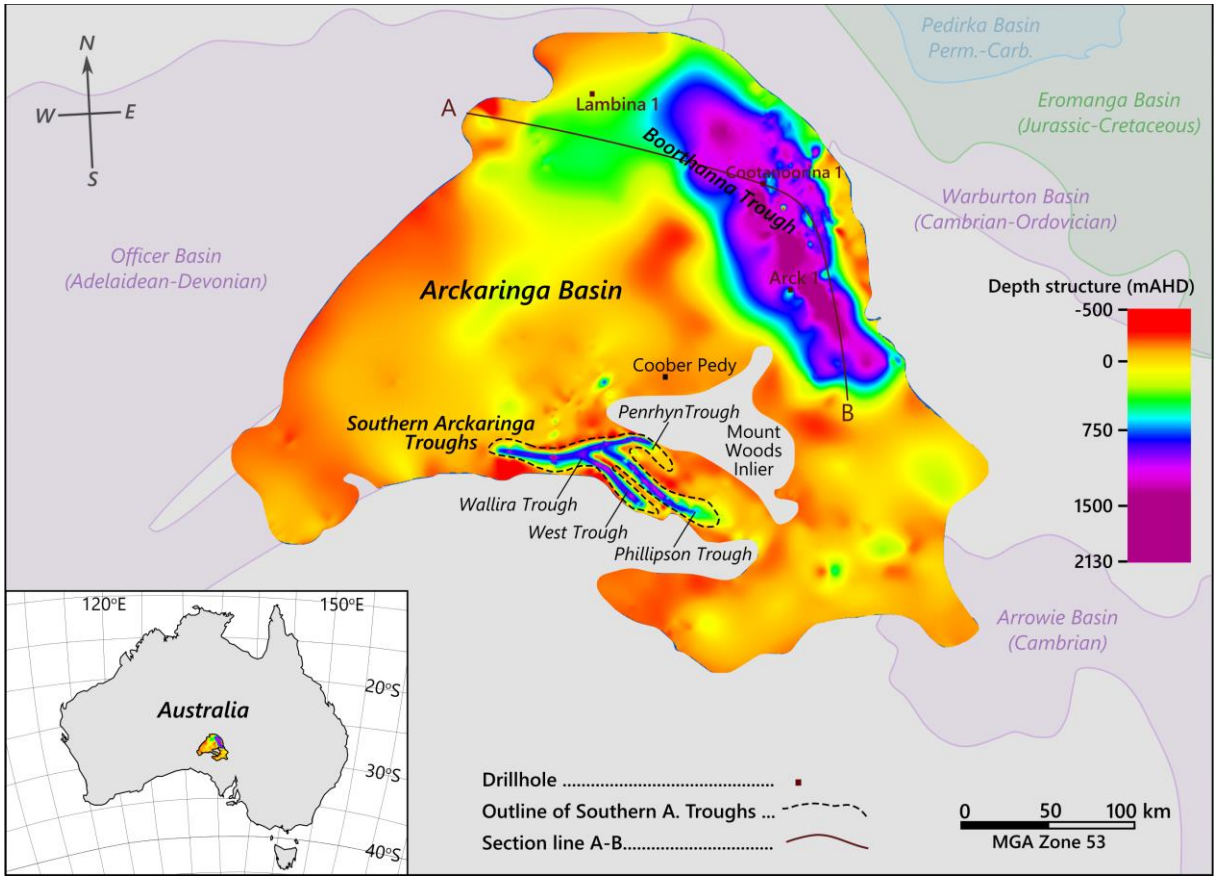

Figure 5: Base Permian depth structure map of the Arckaringa Basin in South Australia, showing the depths of the Boorthanna Trough and Southern Arckaringa Troughs. Note that recent 2D seismic surveys have shown that the Boorthanna Trough extends further southward (Menpes pers. comms.). The locations of Arck 1, Cootanoorina 1, and Lambina 1 within the Boorthanna Trough are also shown, intersected by section line A–B. Modified after Menpes (2013).

Basin Morphology

A review of the basin morphology and identification of sources of geochemical and sedimentological variability across the basin is provided here, drawing on recent seismic profiles and drill cores. The Arckaringa Basin depth structure map identifies a horseshoe-like shape, identifying the broad Boorthanna Trough (up to 90 km wide) to the north-east and the narrow Southern Arckaringa Troughs (5 to 15 km wide) to the south (Figure 5). These depocentres are defined by infill sediments exceeding 1,000 metres in depth. In the Boorthanna Trough, the Permo-Carboniferous succession is partially underlain by early Palaeozoic Cootanoorina Formation and Neopoterozoic sediments of the Adelaide Rift complex. In the Southern Arckaringa Troughs, the succession is underlain by Archaean to Early Mesoproterozoic rocks of the Gawler Craton (Hibburt 1984).

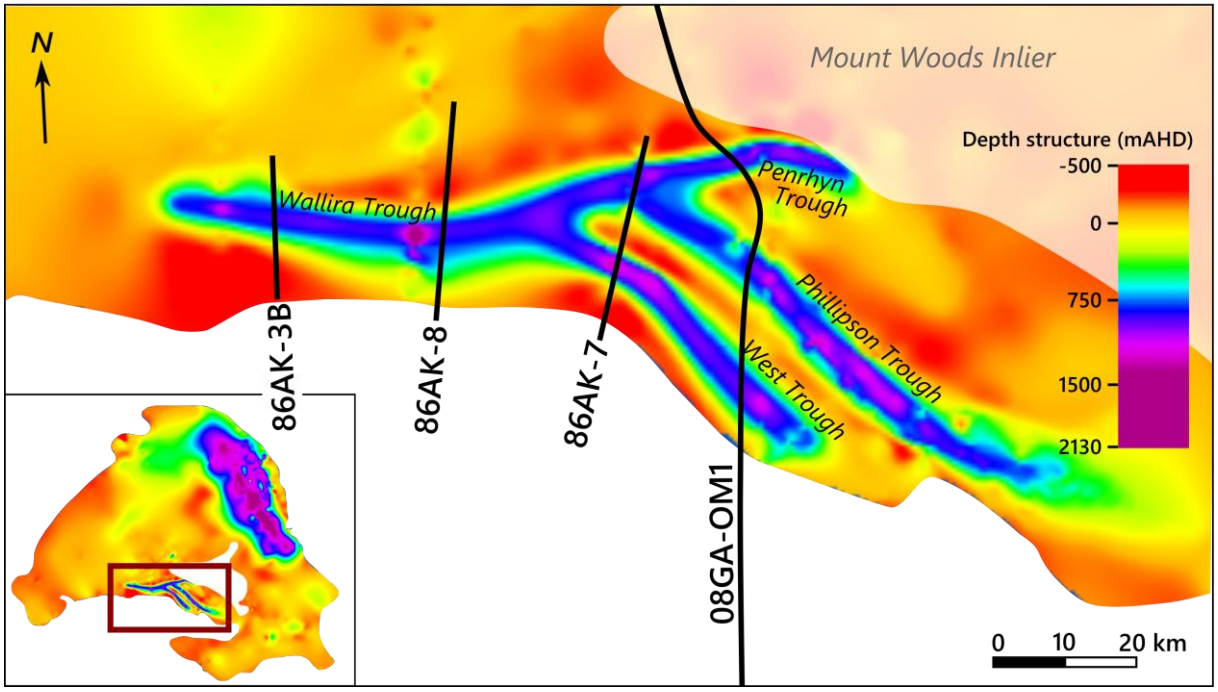

Figure 6: Orientation of seismic lines 86AK-3B, 86AK-8 and 86AK-7 from 1986 and GOMA seismic line 08GA-OM1 from 2008, intersecting the Southern Arckaringa Basin troughs (West Trough, Phillipson Trough, Penryn Trough, and Wallira Trough). Zoomed in base Permian depth structure map from Figure 5, as indicated by red square in inset.

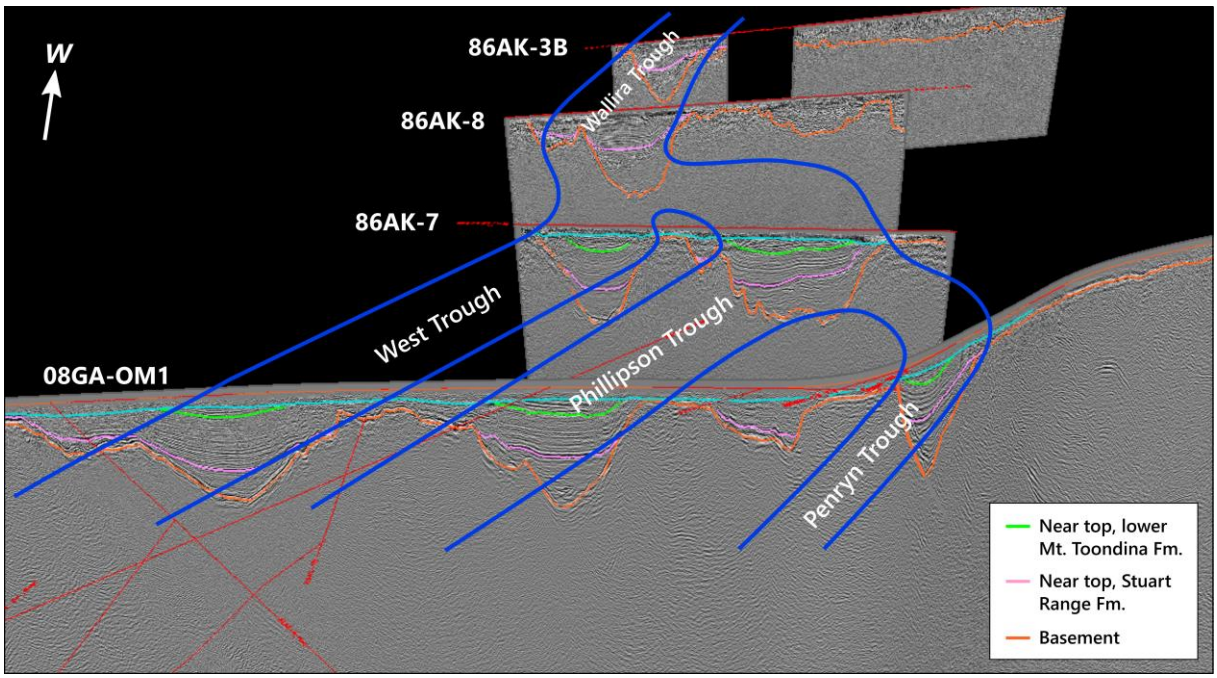

Figure 7: Interpretation of seismic lines 86AK-3B, 86AK-8, and 86AK-7 from 1986, together with 2008 GOMA seismic line 08GA-OM1 of the Southern Arckaringa Basin troughs (West Trough, Phillipson Trough, Penryn Trough, and Wallira Trough), showing the current geometry of the troughs (unflattened). Note the direction of view, perpendicular to Figure 6. The blue line outlines the troughs on the basis of the top of the Mount Toondina Formation. After Menpes *et al.* (2010a).

Seismic data acquired from 1980 to 1989 combined with the 2008 GOMA seismic survey reveals fjord-like steep walled troughs (Southern Arckaringa Troughs; Figure 6 and Figure 7). Seismic interpretations of the West Trough, Phillipson Trough, and Penryn Trough are illustrated in Figure 8, and interpretations of the Wallira Trough are illustrated in Figure 9. The Phillipson and Penryn Troughs are bounded by sub-vertical normal displacement showing stratigraphic onlap, indicating syn-sedimentary extensional faulting. Minor faults are also evident in the West Trough. The Wallira Trough shows a U shaped morphology and is not bounded by faults. Glacial scour likely contributed to the morphology of these troughs, particularly the Wallira Trough, given the U shaped morphology and glacial fill of the Boorthanna Formation (Wopfner 1970; Menpes *et al.* 2010b). The Boorthanna Formation shows strong reflectors in seismic profile (Table 5; Menpes *et al.* 2010a). It varies in thickness across fault blocks and also shows constant thickness in some areas indicating deposition in a broad basin as well as in fault-bounded grabens (Figure 8). Thickening in grabens relative to horst blocks identifies fault subsidence during deposition of the Boorthanna Formation that continued in to the Stuart Range Formation and Mount Toondina Formation. The Stuart Range Formation is weakly reflective in comparison. From study of Arck 1, the contact shows interbedding of glacial sediments that indicates a conformable relationship with the Boorthanna Formation. The Stuart Range Formation onlaps the Boorthanna Formation

as well as the fault-bounded walls. The Stuart Range Formation shows deposition that extends uniformly above grabens, sealing faults indicating deposition during thermal relaxation as well as thickening within footwalls of graben to identify continued syn-sedimentary subsidence (Figure 8). The overlying Mount Toondina Formation is not directly affected by faulting, showing broader subsidence across multiple grabens consistent with thermal relaxation. The top of the Permo-Carboniferous succession has been eroded away indicating basinal inversion, and there is a sharp contact between basin sediments and an abbreviated succession of Eromanga Basin and Lake Eyre Basin sediments. This indicates that the overlying sedimentary fill may have been thicker prior to the Mesozoic and enhanced thermal maturity.

In the Boorthanna Trough reflectors interpreted to be the Stuart Range Formation by Menpes (2013), based on sequence stratigraphy, show regional discordant reflectors interpreted to be an unconformity (Figure 10). However, this is not apparent in Arck 1 where an interbedded (conformable) contact is evident, and is also not apparent in the Southern Arckaringa Troughs. Possible explanations include interglacial unconformities resulting from glacial erosion within the Boorthanna Formation. Interpretation of reflectors is difficult given the limited borehole control, so that assignment of specific reflectors is tentative. Downlap of clinoforms on to a conspicuous surface are interpreted as prograding highstand system tract of the Mount Toondina Formation deposited on a maximum flooding surface of the Stuart Range Formation (Figure 10).

The early Palaeozoic Cootanoorina Formation unconformably underlies the Permo-Carboniferous succession within the Boorthanna Trough. It comprises a shallow marine siliciclastic to dolomitic and anhydritic sequence, and is laterally equivalent to the early Cambrian Ouldburra Formation of the Officer Basin (Jones 1988; Hibburt 1995). The formation was deposited as a shallow marine and evaporitic tidal flat sequence on gently undulating Neoproterozoic sediments of the Adelaide Rift complex, and is laterally pervasive (Moore 1982). This suggests that basin formation and major topography development must have occurred after deposition during the early Cambrian.

Table 5: Reflector characteristics used for the interpretation of each formation in seismic profiles, defined by Menpes *et al.* (2010b) based on drill core correlations.

Formation	Reflector characteristics
Upper Mount Toondina Formation	Subparallel reflections
Lower Mount Toondina Formation	Strong subparallel reflections
Stuart Range Formation	Weak reflections
Boorthanna Formation	Strong, irregular reflections

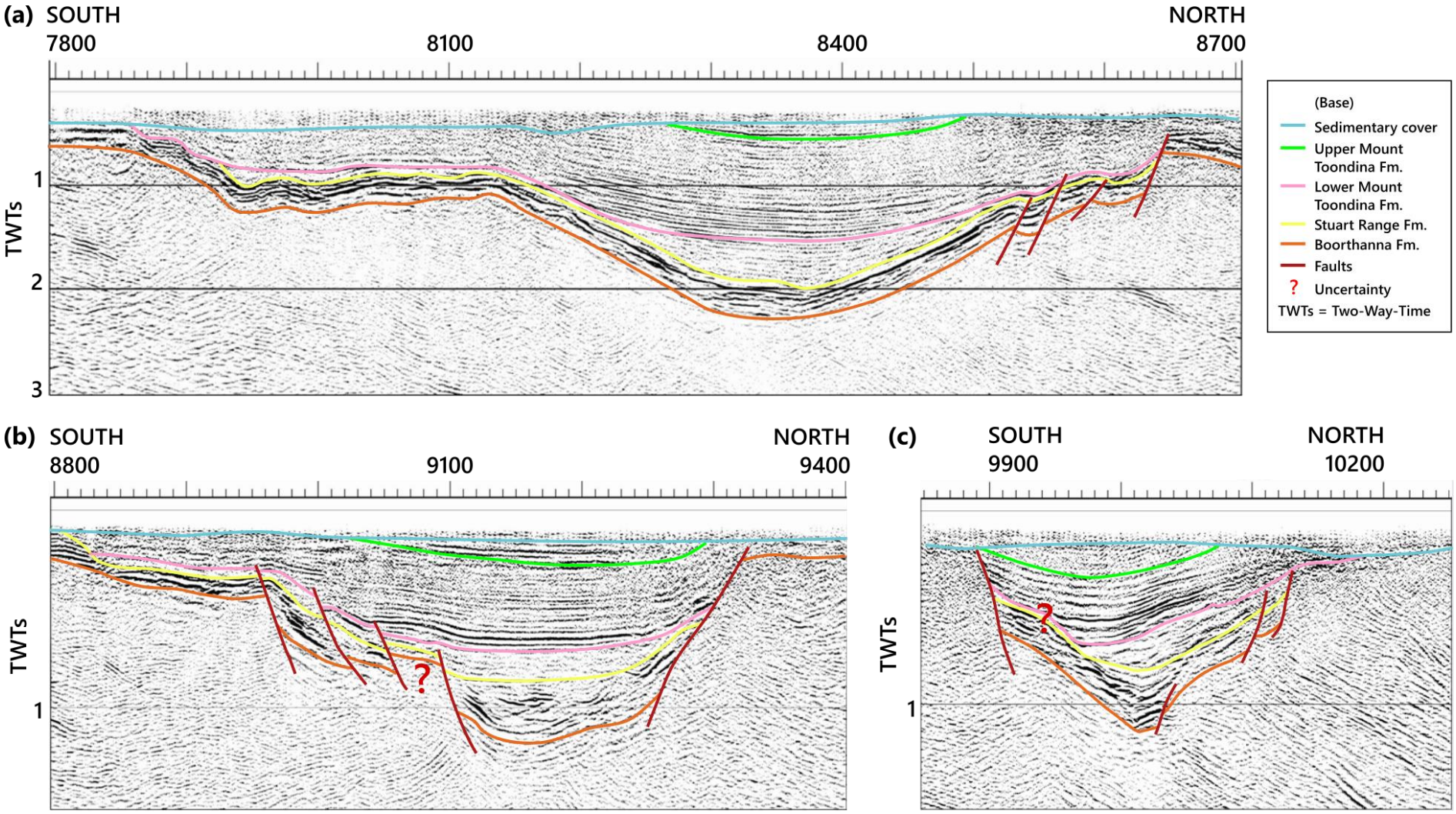

Figure 8: Interpretation of 2008 GOMA seismic line 08GA-OM1 of (a) the West Trough, (b) the Phillipson Trough, and (c) the Penryn Trough. Location of seismic profiles mapped in Figure 6 and shown in Figure 7. Seismic profiles modified after Menpes *et al.* (2010a).

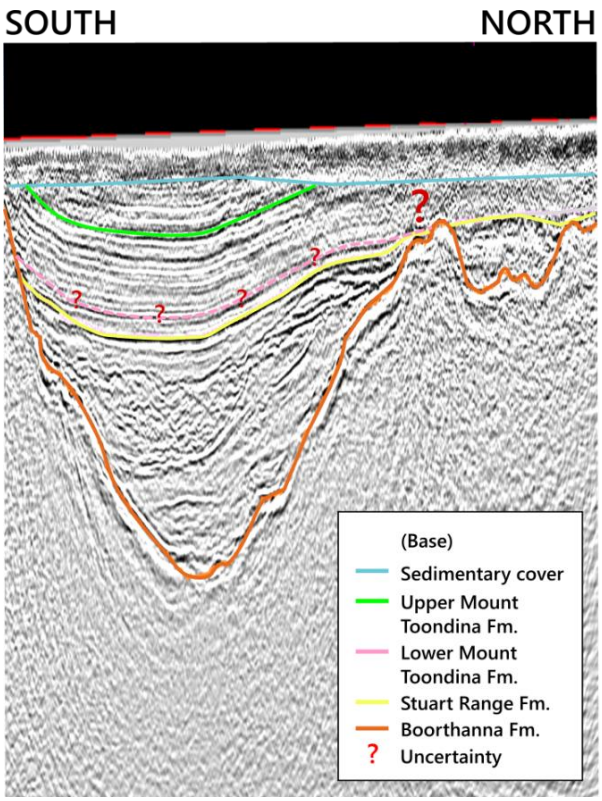

Figure 9: Interpretation of 1986 seismic line 86AK-3B of the Wallira Trough. This seismic identifies steep walls that are not fault-bounded. Location of this seismic profile is mapped in Figure 6 and shown in Figure 7. Seismic profile modified after Menpes *et al.* (2010a).

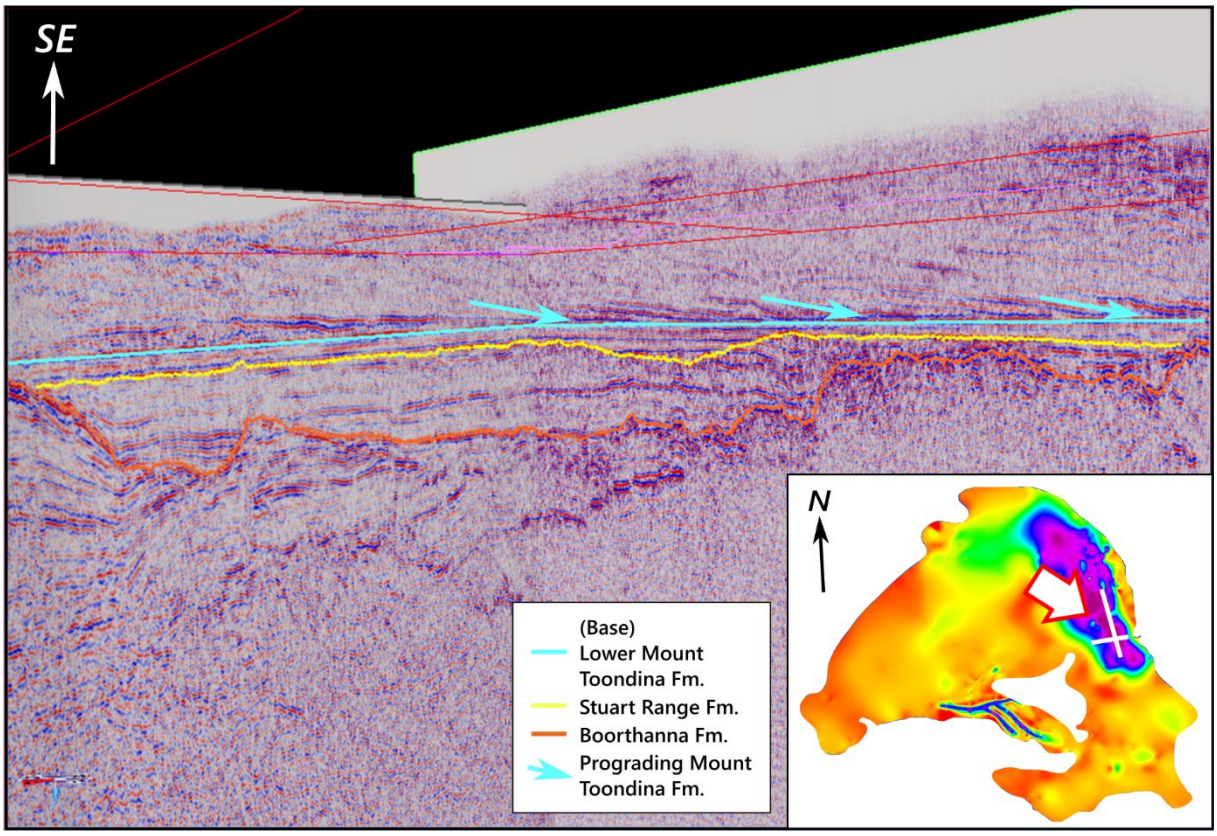

Figure 10: Interpretation of seismic lines 84-XER_mig_08SX (north–south) and 84-XES (west–east), shown by white lines in inset, of the Boorthanna Trough. Red–white arrow in inset points to the view of seismic lines illustrated here. The Mount Toondina Formation progrades on to the Stuart Range Formation from the east as indicated by the blue arrows. Interpretations have been made by Menpes (2013) on the basis of sequence stratigraphy.

Sediments of the Stuart Range Formation from Arck 1 core

The Stuart Range Formation has the greatest source rock potential and was studied in Arck 1, Cootanoorina 1, and Lambina 1 cores to determine depositional environment, depositional controls, and palaeoceanographic influences on mineralogy and organic matter content. In general, it is an organic-rich feldspathic micaceous siltstone that is mineralogically immature (Figure 11). A study of the Arck-1 core revealed four facies (Figure 12 and 13) in the Stuart Range Formation reflecting pelagic deposition under different basin water chemistry and redistribution from mass flows. Total organic carbon (TOC) was significantly enhanced between pelagic deposits and mass flow deposits. Mineralogy varied at micron scale within the pelagic sediments (Table 6). The Arck 1 core was studied in greatest detail, with broad sampling of facies to characterise mineralogy and organic carbon properties followed by more detailed study of laminated pelagic intervals (Figure 12). The four facies are described below.

PROGLACIAL FACIES

The Proglacial Facies is confined to the basal 12 m of the Stuart Range Formation. It is a laminated mudstone due to mineralogy variation (1 cm laminations), with thin interbeds of fine grained sandstone. It contains isolated sub-angular to rounded igneous and meta-igneous pebbles or lonestones (<4 mm to 20 mm). Isolated pebbles to cobbles are present throughout the facies (< 1/m) causing soft sediment deformation of mudstone, and are interpreted as dropstones (Figure 13) resulting from ice rafting in glacial conditions. X-ray diffraction (XRD) identified clays, quartz, feldspars, carbonates, jarosite, chlorite, and pyrite. Carbonate phases include dolomite and kutnohorite, and clay phases include illite/mica, kaolinite and chlorite. Table 6 summarises the mineralogy of the four facies based on bulk powder XRD and shows the percentage of samples within each facies that contain a given mineral. The two Proglacial Facies samples analysed showed consistent mineralogy, containing a high proportion of silicates with minimal carbonates. The presence of dropstones indicates the continuation of glacial conditions from the Boorthanna Formation into the Stuart Range Formation. It therefore associates cold climate environmental depositional conditions with the organic carbon enrichment characteristic of the Stuart Range Formation. This implies that there was no time break with deposition of the Boorthanna Formation, making truncated seismic reflectors interpreted to represent a sequence boundary problematic.

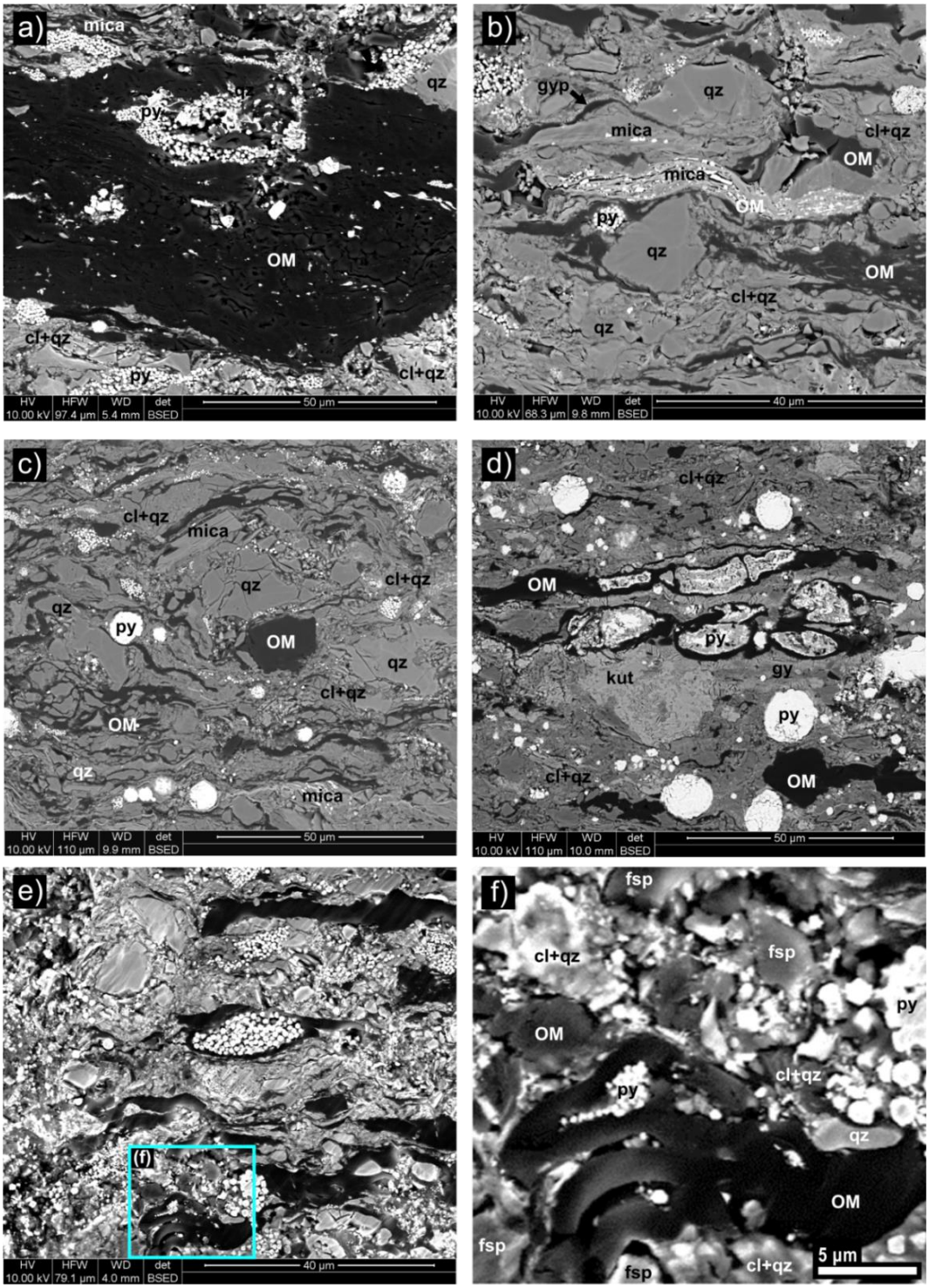

Figure 11: Scanning electron microscope (SEM) photomicrographs showing the compositionally immature nature of the detrital mineral component within the Stuart Range Formation and its relationship to organic matter (OM). OM is bounded by sub-angular quartz (qz) grains and detrital mica surrounded by a clay and quartz (cl+qz) matrix that is likely dominated by illite and kaolinite. Altered mica grains show extensive fraying and contain pyritic (py) replacement. Gypsum (gyp) within close proximity of OM is also apparent, though this is likely to date post-core extraction. Kutnohorite (kut) is observed in some samples. (a) Sample 2053188 (Massive Black Shale, TOC: 8.18); (b) 2053194 (Cyclic Varve Unit, TOC: 3.04); (c) 2053196 (Massive Black Shale, TOC: 7.74); (d) 2053198 (Lensed Mudstone, TOC: 4.64); (e) OM-rich sample (2053191 Massive Black Shale, TOC: 8.24) with sporinite and minor lamalginite; and inset (f) indicating no association between OM and diagenetic components, which are only minor in the high TOC samples.

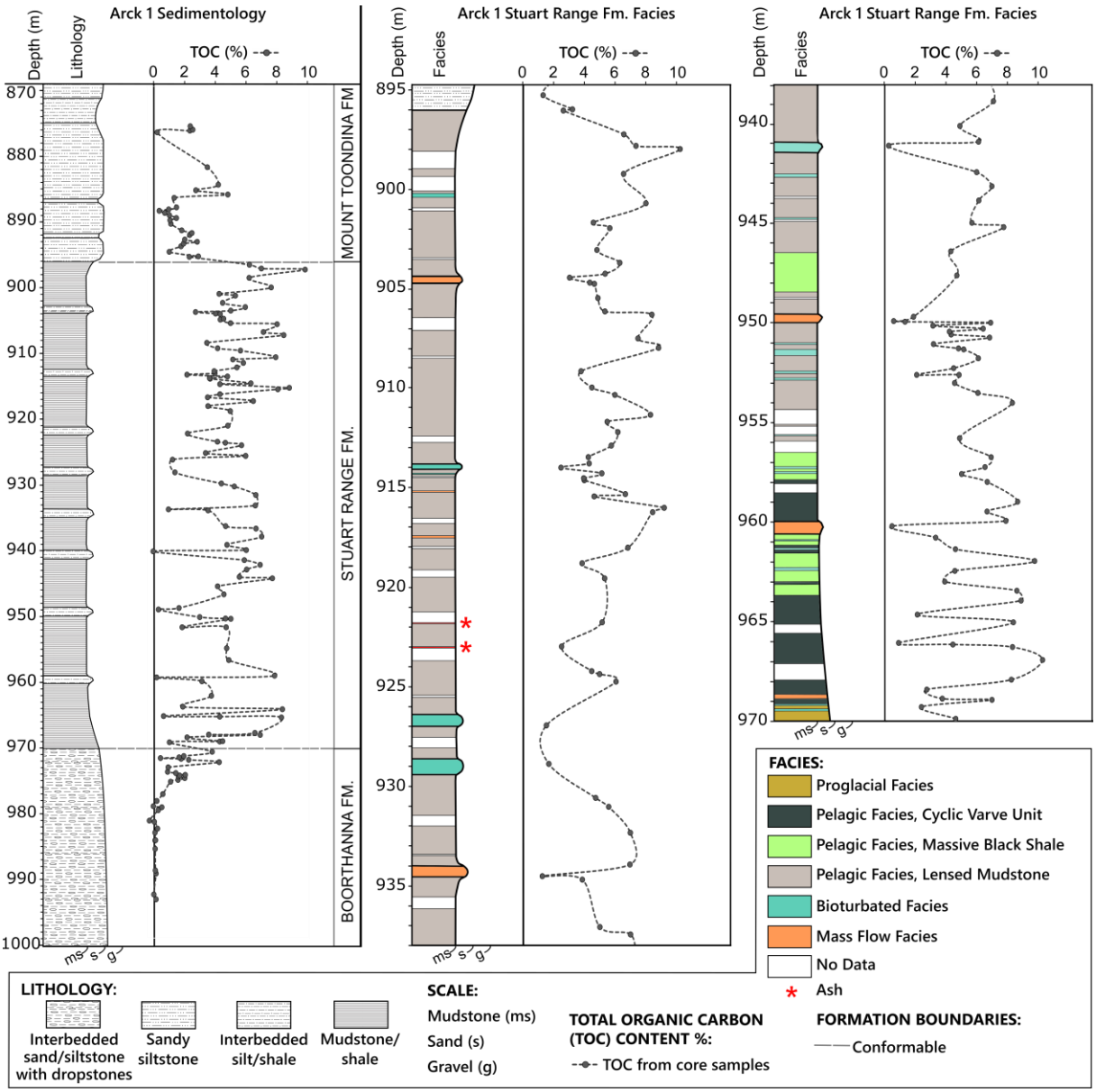

Figure 12: Core log of Arck 1 illustrating lithological and geochemical variability (left), with total organic carbon (TOC) data from core samples plotted against depth. The Arck 1 core log comprises the upper Boorthanna Formation, the Stuart Range Formation, and the lower Mount Toondina Formation. The heterogeneous Stuart Range Formation was studied (right) and four facies were identified. The Pelagic Facies sub-facies are shown here. Thin ash layers (approximately 2 cm thick) are indicated by red asterisks. Note that the subsection depth scale is three times the Arck 1 core log depth scale.

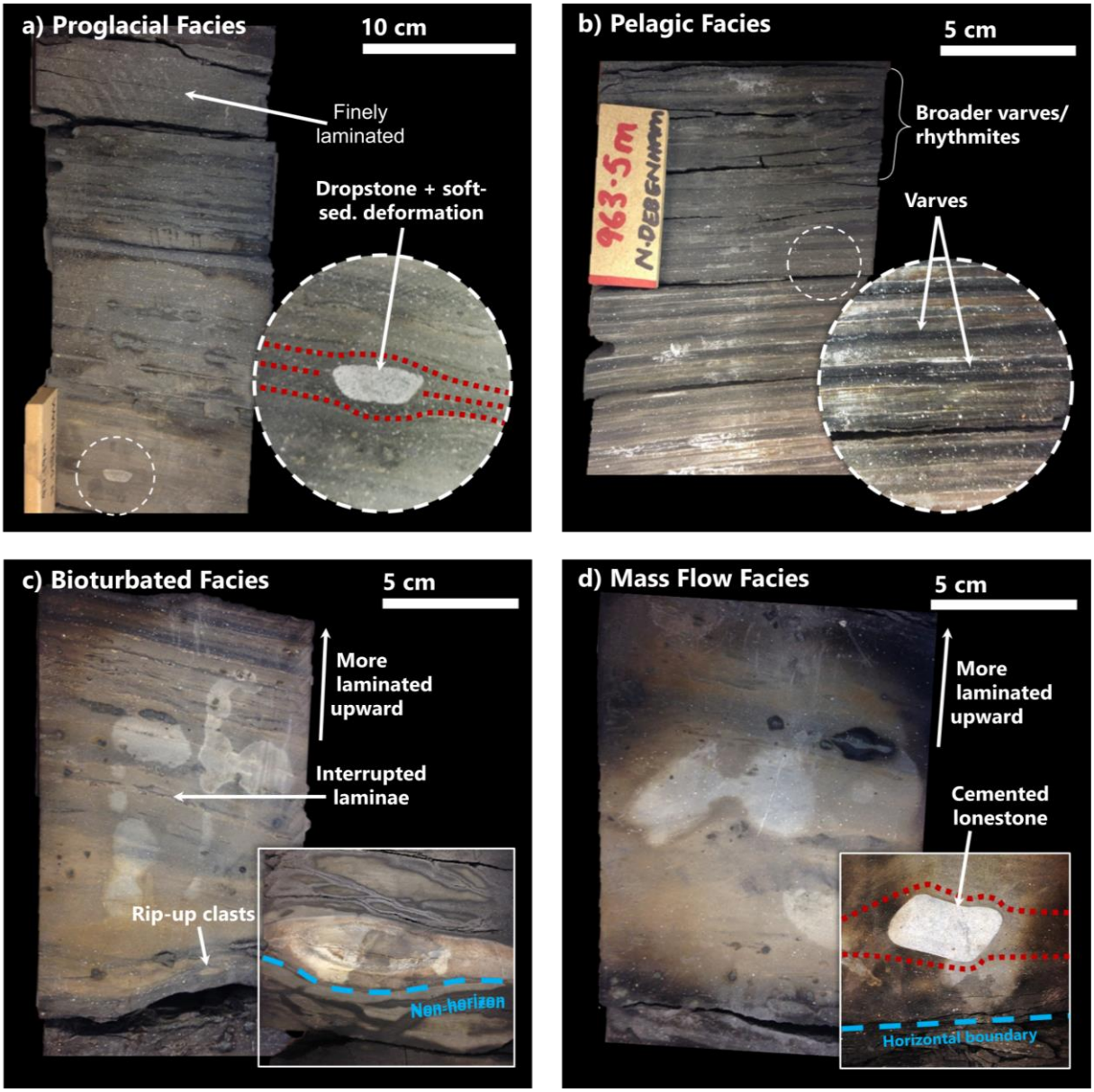

Figure 13: Representative images and characteristic features of the four facies identified within the Stuart Range Formation, Arck 1, at core scale: (a) Proglacial Facies, (b) Pelagic Facies, (c) Bioturbated Facies, and (d) Mass Flow Facies.

Table 6: Typical mineralogy of the four facies identified within the lower Stuart Range Formation, X-ray diffraction (XRD) of bulk powders (Appendix B, Table B1 and B2). The three sub-facies identified within the Pelagic Facies have also been included. The presence (%samples) of mineral phases has been grouped into 'all samples', 'most samples', and 'few samples'. 'N/A' has been assigned to facies with only 2 XRD sample results. The number of XRD samples is bracketed beside each facies number.

	Typical Mineralogy (Presence %samples in XRD Samples)		
Facies	All samples (100%)	Most samples (99–31%)	Few Samples (<30%)
Proglacial Facies (2)	Quartz, albite, illite/mica, K-feldspar, kaolinite, chlorite, kutnohorite, jarosite, pyrite	Dolomite	N/A
Pelagic Facies (2) Cyclic Varve* Unit	Quartz, albite, illite/mica, kaolinite, jarosite, gypsum, pyrite, chlorite	Dolomite, kutnohorite, apatite	N/A
Pelagic Facies (5) Massive Black Shale	Quartz, albite, illite/mica, kaolinite, jarosite, gypsum, pyrite	Chlorite	K-feldspar
Pelagic Facies (3) Lensed Mudstone	Quartz, albite, illite/mica, kaolinite, jarosite, gypsum, pyrite	K-feldspar	Mixed I-S, kutnohorite, apatite
Bioturbated Facies (2)	Quartz, illite/mica, kaolinite, dolomite, apatite	Albite, K-feldspar, chlorite, magnesite, kutnohorite, jarosite, gypsum, pyrite	N/A
Mass Flow Facies (2)	Quartz, albite, kaolinite, chlorite, siderite, dolomite, kutnohorite, pyrite	Magnesite, jarosite	N/A

*Evidence for finely laminated varve is provided later in thesis.

PELAGIC FACIES

The Pelagic Facies is the most pervasive facies within the Stuart Range Formation. This facies has been divided into three sub-facies (Figure 14) which are mineralogically and texturally similar, implying a common detrital source and depositional setting. Each sub-facies is detailed in subsequent sections below. The Pelagic Facies contains repetitive asymmetrical laminations (0.001 to 1 cm) of light and dark sediments (detailed below). Due to the absence of gravitational reworking, these laminations formed from episodic periods of settling, and thus this facies it is interpreted to represent background pelagic settling. The Pelagic Facies provides an opportunity to study the relationship of depositional environment on OM preservation that can support palaeoceanographic models explaining variations in source rock properties in the Arckaringa Basin.

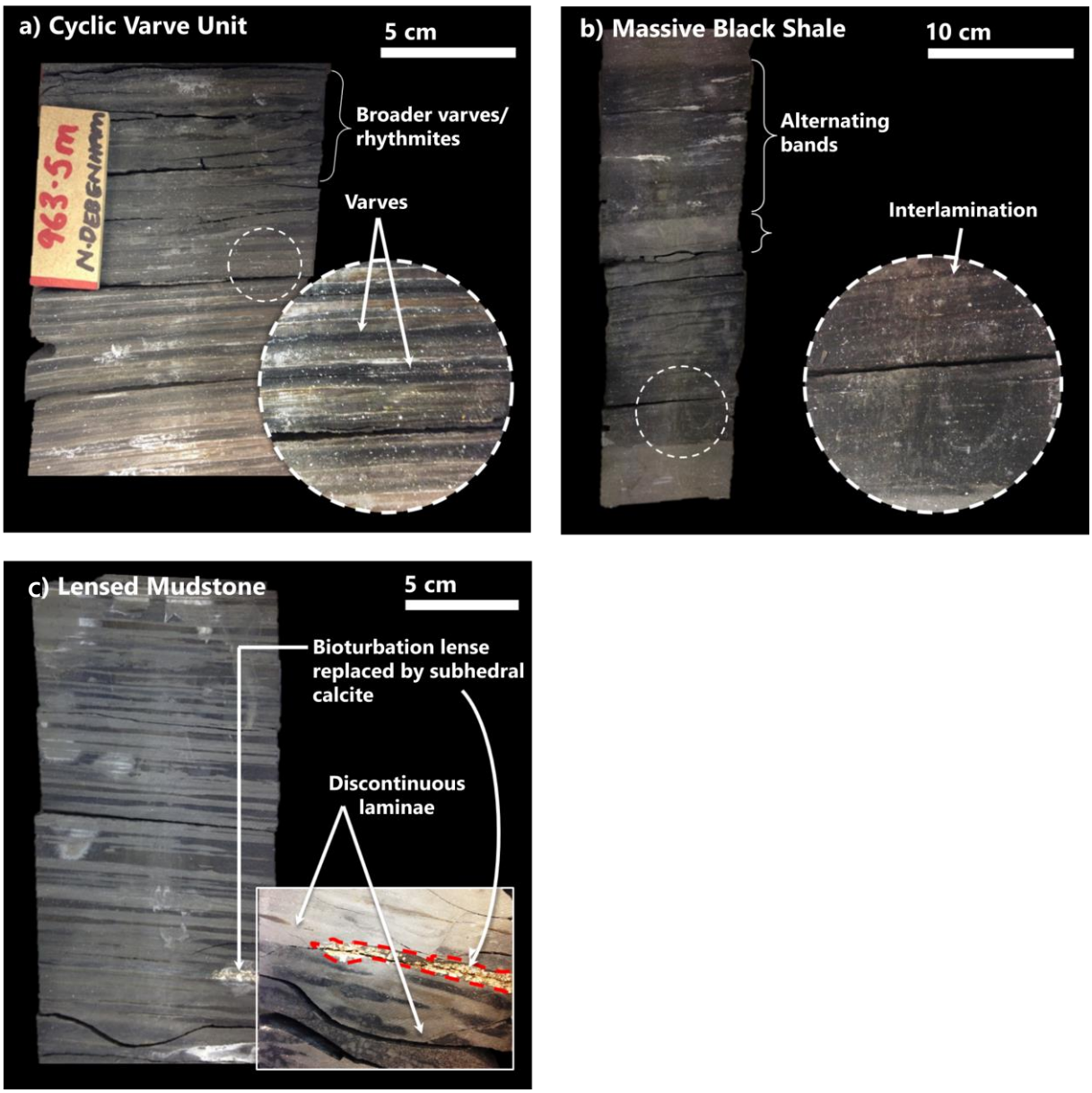

Figure 14: Representative images and characteristic features of the three Pelagic Facies sub-facies identified within the Stuart Range Formation, Arck 1, at core scale: (a) Cyclic Varve Unit, (b) Massive Black Shale, and (c) Lensed Mudstone.

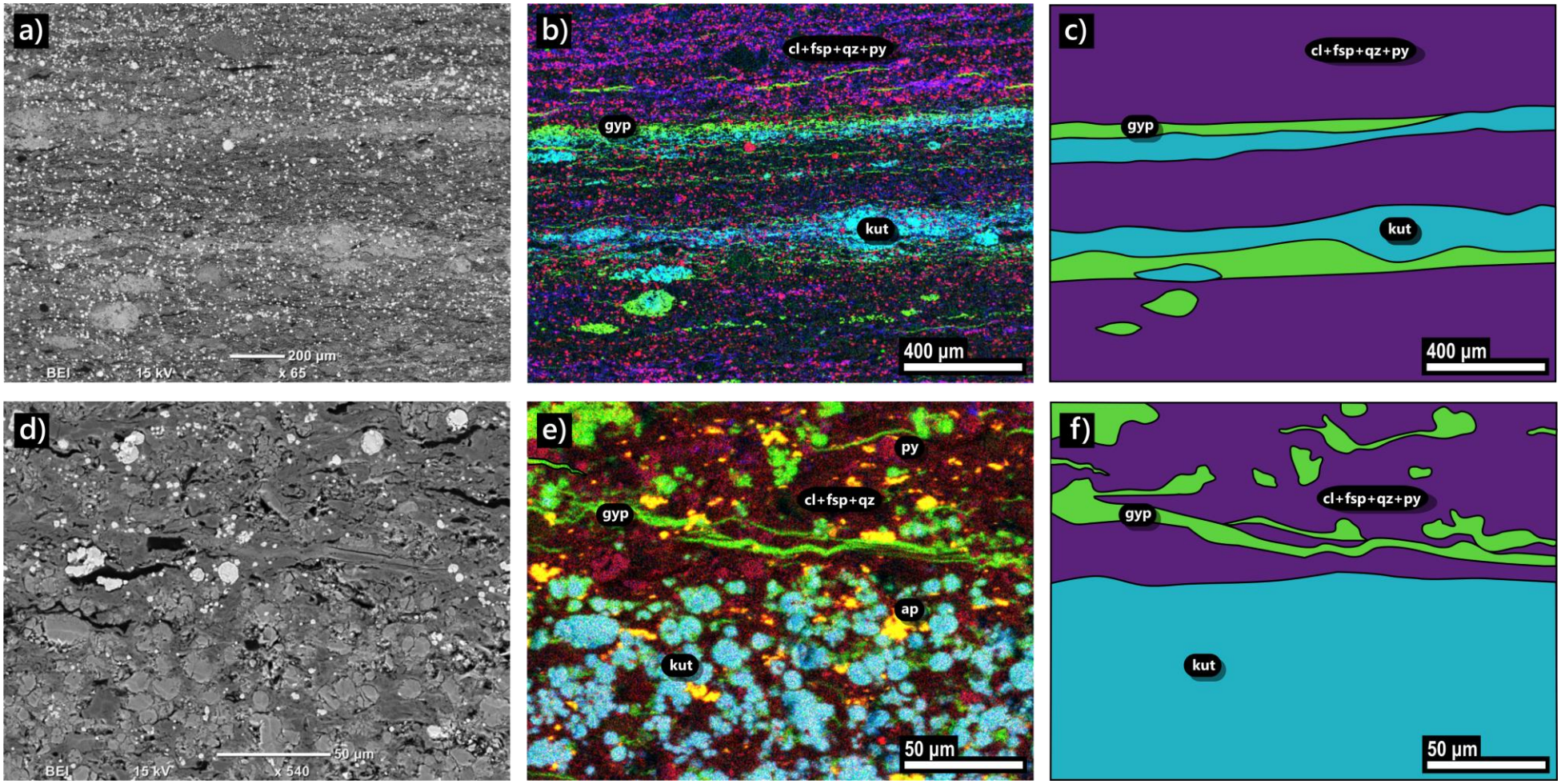

Figure 15: Scanning electron microscope (SEM) and integrated energy dispersive X-ray spectroscopy (EDS) photomicrographs of polished blocks taken from the Pelagic Facies in the Stuart Range Formation in Arck 1, where red = silicon, green = calcium, and blue = manganese. The important minerals identified are gypsum (gyp) and kutnohorite (kut), surrounded by a primarily clay, feldspar, and quartz (cl+fsp+qz) matrix with framboids of pyrite (py) and apatite (ap). Note the scale difference. (a) SEM photomicrograph of sample 2053196 at 959.97 m (Massive Black Shale), (b) accompanying EDS map of elemental distributions, and (c) cartoon drawing of EDS map, showing dominant mineralogy. (d) SEM photomicrograph of sample 2053198 at 955.79 m (Lensed Mudstone), (e) accompanying EDS map of elemental distributions, (f) cartoon drawing of EDS map, showing dominant mineralogy.

Energy-dispersive X-ray spectroscopy (EDS) coupled with BSEM was used to map the distribution of mineral phases including minor mineral phases that were not detected from XRD. Mineral distribution mapping, by integrating EDS with BSEM, identified repetitive kutnohorite bands (manganese carbonate) separated by a clay, feldspar, quartz, and pyrite matrix zone (Figure 15). At the interface of each kutnohorite band, gypsum was identified (a diagenetic mineral likely post-dating core extraction). The pale kutnohorite bands vary in thickness (0.001–0.1 cm) reflecting the degree of oxic bottom water conditions and associated bioturbation that is inducing these differences (detailed below). The Cyclic Varve Unit comprises the most pronounced and pervasive rhythmicity of all three sub-facies. Subsequent XRD identified varying abundances of quartz, pyrite, illite/mica, kaolinite, chlorite, and K-feldspar within the darker laminae, and quartz, kutnohorite, dolomite, jarosite, and gypsum within the lighter laminae. XRD analysis of clay separates (Figure 16) of each sub-facies indicated the presence of illite, smectite (presence uncertain in the Cyclic Varve Unit), mixed layer illite-smectite (identified using ethylene glycol treatment), kaolinite, and chlorite.

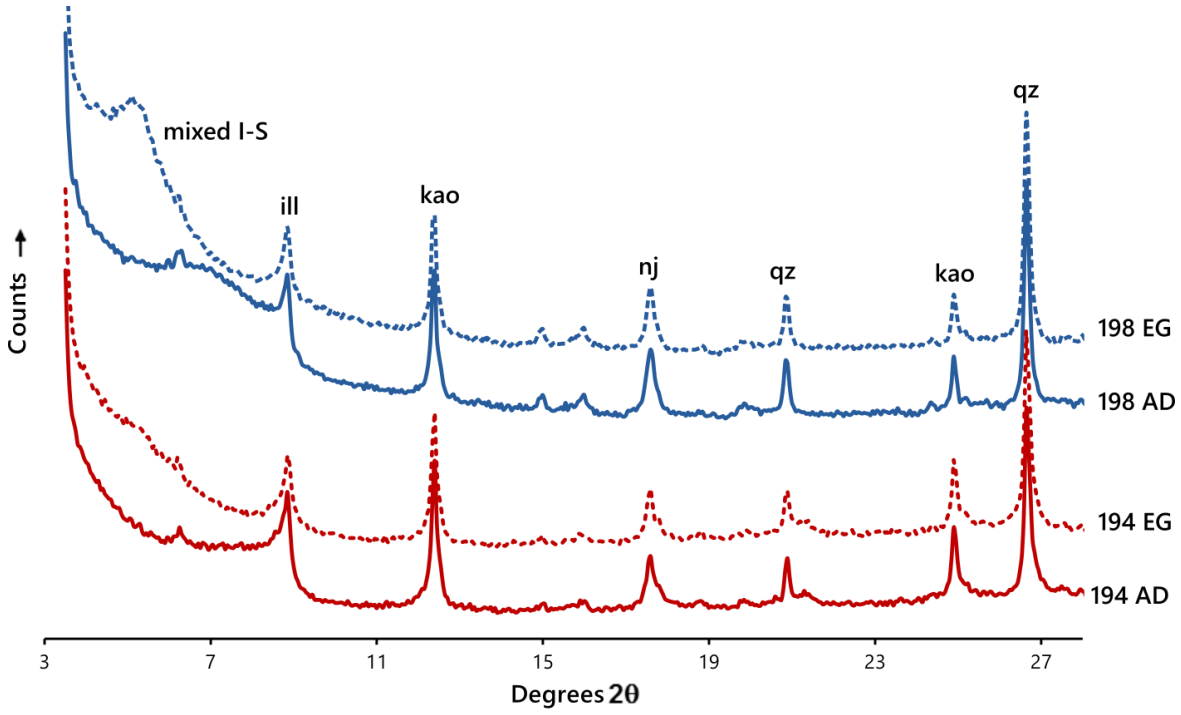

Figure 16: Clay mineral fraction X-ray diffractogram of Arck 1 Pelagic Facies (Massive Black Shale) samples 2053194 (red) and 2053198 (blue), with both air dried (solid line) and ethylene glycol (dashed line) treatments. The diffractograms have been shifted upwards for clarity. Mixed layer illite-smectite (mixed I-S), illite (I), kaolinite (kao), natrojarosite (nj), and quartz (qz) were identified. Data based on Appendix B, Table B1. The phyllosilicate mineral compositions were determined by applying the United States Geological Survey (USGS) Clay Mineral Flow Diagram of Poppe *et al.* (2001).

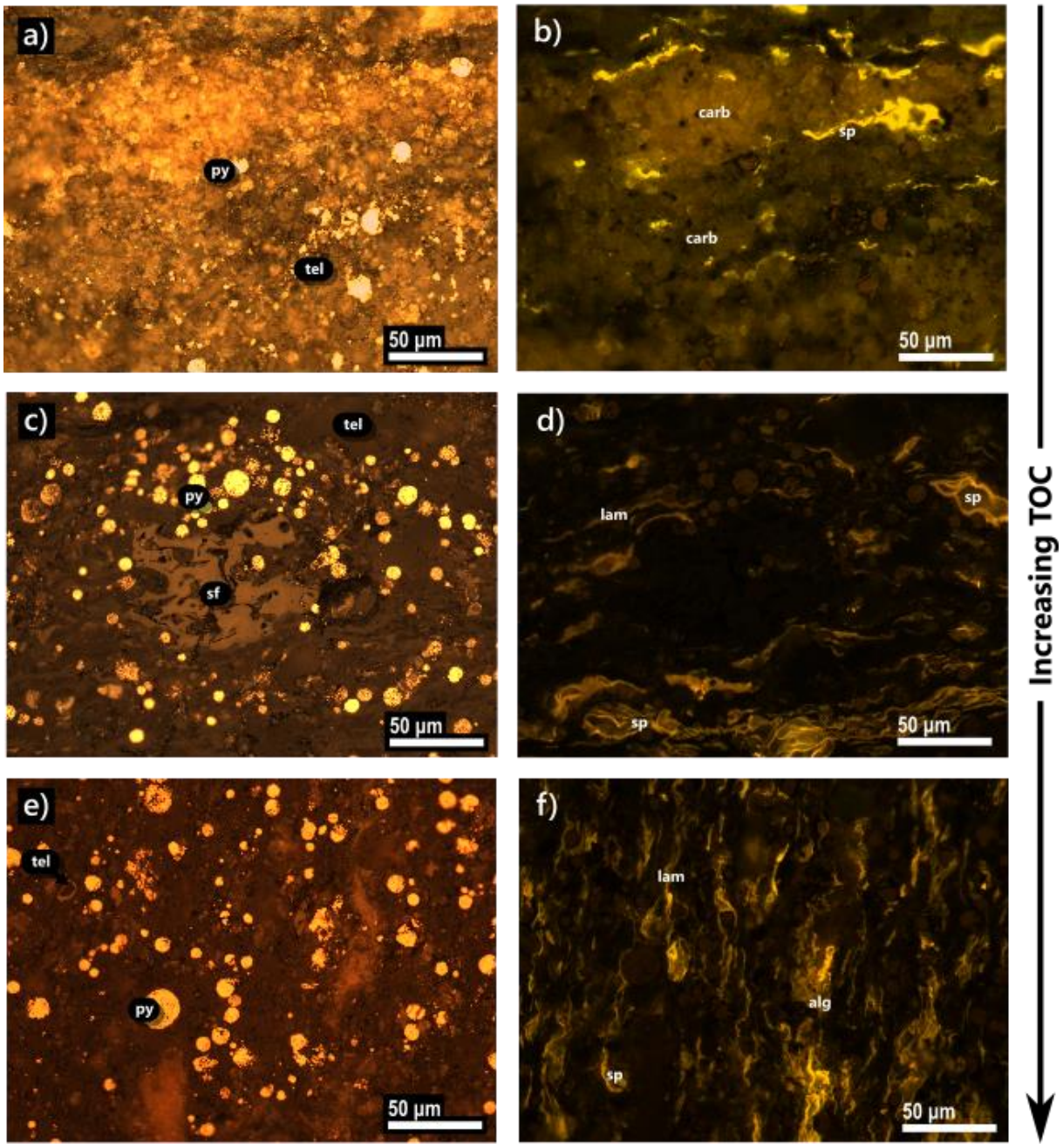

Figure 17: Reflected light (left) and ultra-violet (right) photomicrographs showing the organic components within the Stuart Range Formation Pelagic Facies, from low Total Organic Carbon (TOC) contents to high. (a, b) Sample 2053194 at 960.82 m, bulk TOC = 3.04, Cyclic Varve Unit. A high proportion of carbonates are present, which is typical of low TOC samples. This image captures a Mn carbonate laminae. Comprises fine telinite (tel, terrestrial OM) with minor sporinite (sp), also of terrestrial origin. (c, d) Sample 2053197 at 957.60 m, bulk TOC = 4.78, Cyclic Varve Unit. This image captures the organic-rich laminae. Semifusinite (sf) surrounded by abundant sporinite, framboidal pyrite (py), lamalginite (lam), and minor telinite. (e, f) Sample 2053196 at 959.97 m, TOC = 7.74, Massive Black Shale. Abundant lamalginite, sporinite, and framboidal pyrite, with minor alginite (alg) and telinite. Lamalginite, alginite, and framboidal pyrite are of marine origin. The classification table for the identification of organic macerals in in the methods chapter was followed during analysis.

Petrographic observations of the Pelagic Facies in fluorescence and reflected white light mode indicated a predominance of liptinite, with sporinite (terrigenous origin), alginite, and lamalginite (both marine origin) as the main macerals (Figure 17). Spores (sporinite) were typically 20 µm sized ellipsoidal shapes with thick, distinct walls and quartz, clay, and pyritic centres. These were often deformed, likely due to burial compaction. Alginite had a 'cauliflower' appearance suggesting algal colonies of up to 50 µm. Long and string-like, thin-walled lamellar OM was identified as lamalginite. Due to the spindly nature of this maceral and how it appears to wrap around mineral grains, it is possible that migrated hydrocarbon phases could be confused with lamalginite. Other terrigenous macerals include semifusinite (broken fragments of plant wall) and telinite (tabular woody tissue) which occur as angular fragments 10 µm to 50 µm. Typically, samples with lower TOC values are dominated by terrigenous OM, i.e. vitrinite and sporinite (Figure 17a and b), and samples with higher TOC values are dominated by abundant lamalginite, alginite, and sporinite (Figure 17e and f).

Unlike the OC-rich (organic carbon) shales accumulating during greenhouse periods with OC that is intimately associated with fine-grained chemically mature sediment, there is no obvious textural association between the OM and the diagenetic components in the Stuart Range Formation (Figure 12). BSEM imaging of the Pelagic Facies indicates a poorly sorted, compositionally and texturally immature, feldspathic micaceous siltstone (Figure 12). Sub-angular to sub-rounded quartz grains and detrital mica are surrounded by a silica-rich matrix, dominated by illite/smectite, kaolinite, and mm-scale authigenic quartz. These were also identified by EDS mapping and point analysis and XRD. Framboidal and euhedral pyrite comprise up to 20 wt% of the organic-rich intervals (Figure 18). Authigenic gypsum is present in the darker laminae, where it is often spatially associated with OM particles. TOC is higher in finer grained sediments within the darker laminae, which may simply reflect reduced dilution by siliclastic phases. EDS spot analysis of discrete OM particles (Figure 19) showed that the OM contains variable quantities of sulphur (S). Greater concentrations of S were identified within more labile sporinite and lamalginite, and minor amounts of S within vitrinite group macerals, predominantly telinite.

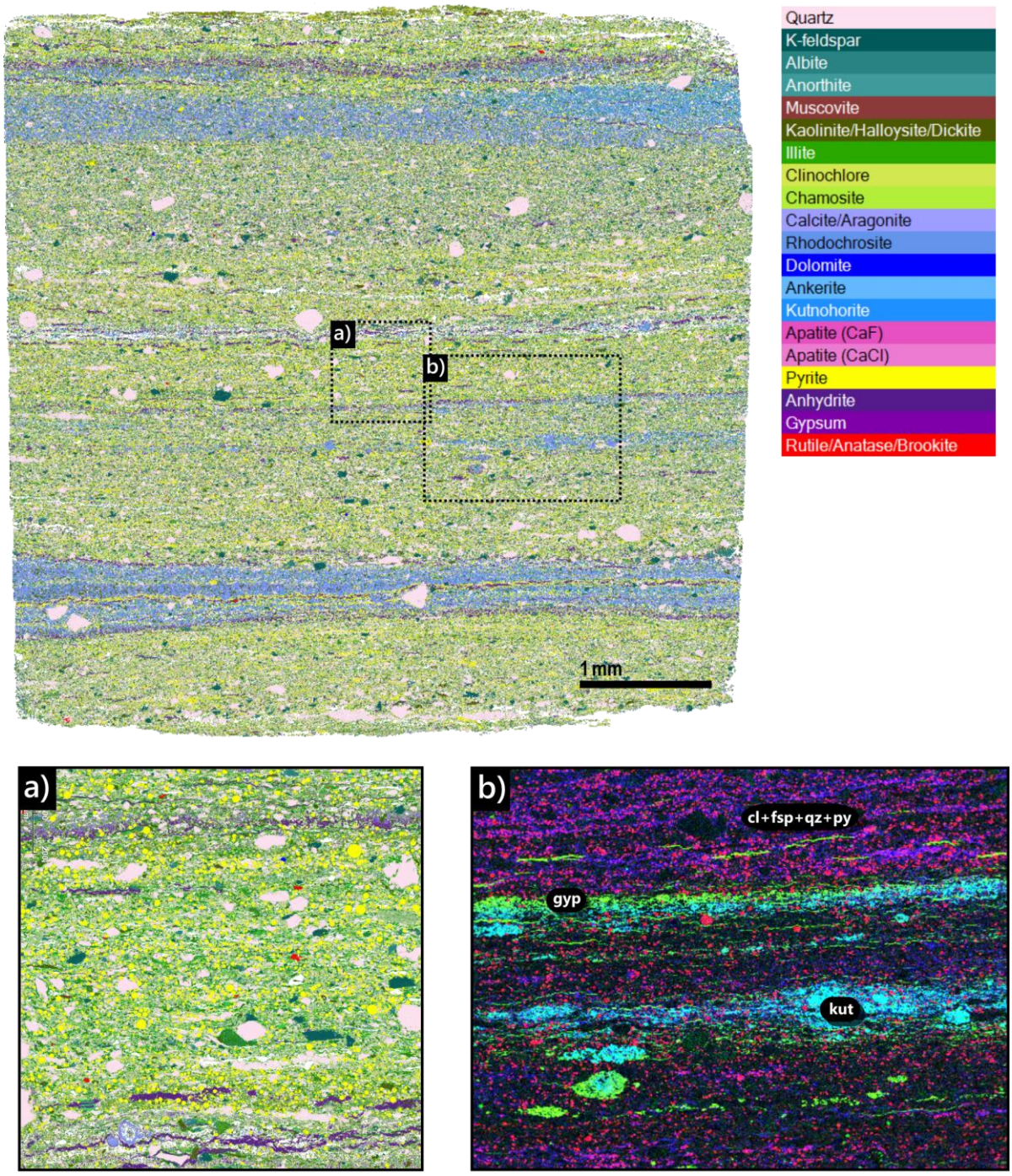

Figure 18: Quantitative Evaluation of Minerals by Scanning electron microscopy (QUEMSCAN® by FEI Company) mineral map of a polished block taken from the Massive Black Shale in Arck 1 (sample 2053196 at 959.97 m) using energy-dispersive X-ray spectroscopy (EDS) for data acquisition. The legend (right) illustrates the colour assignment of the minerals present. (a) This mineral map inset further details mineral associations and distributions. The repetitive laminae (50–800 µm width) illustrated by the blue–purple shades that primarily represent gypsum ± anhydrite (purple), and rhondochrosite (± anhydrite), and kutnohorite (blue). This also demonstrates the compositionally immature nature of the detrital mineral component within the Stuart Range Formation, with sub-angular to sub-rounded quartz grains, poorly sorted K-feldspar, and detrital mica surrounded by a clay and quartz matrix dominated by illite and kaolinite. (b) EDS map of elemental distributions from Figure 15b. Note the colour scheme of this inset is not represented in the legend. This inset shows how fine the laminae can be throughout the Pelagic Facies.

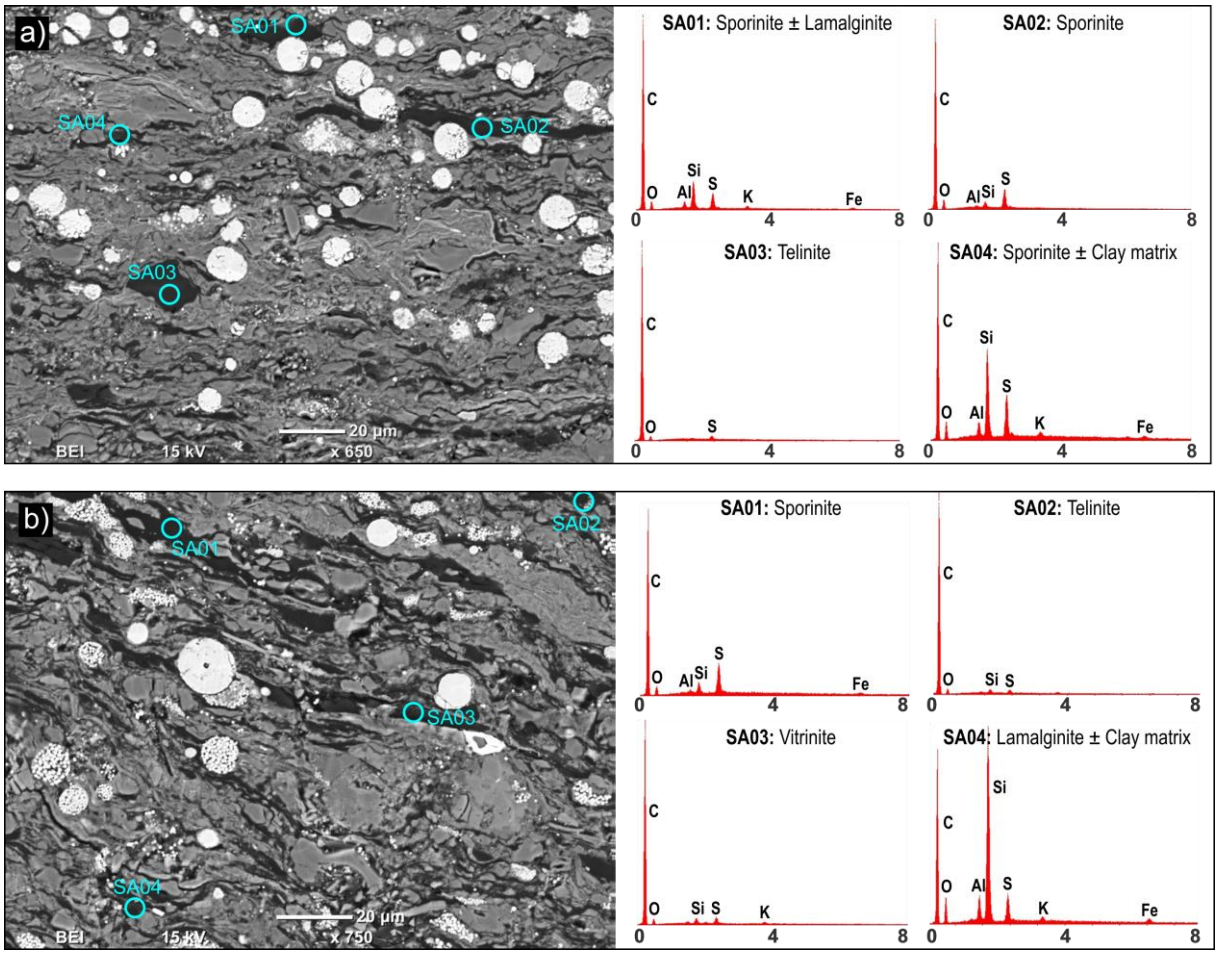

Figure 19: Scanning electron microscope (SEM) photomicrograph of polished blocks from the Massive Black Shale (Pelagic Facies) within the Stuart Range Formation, Arck 1. Energy dispersive spectroscopy (EDS) spot analysis within discrete particles of organic matter was performed to determine elemental compositions. The peaks are illustrated graphically to the right. Peaks indicate the presence of carbon (C), oxygen (O), aluminium (A), silicon (Si), sulphur (S), potassium (K) and iron (Fe). 'Clay matrix' indicates where spot analysis has also analysed the clay matrix. Representative samples are shown here: (a) 2053196 at 959.97 m, total organic carbon (TOC): 7.74, and (b) 2053188 at 966.35 m, TOC: 8.18, sub-facies 2b. Greater concentrations of S were identified within more labile sporinite and lamalginite, and minor amounts of S within vitrinite group macerals, predominantly telinite.

Cyclic Varve Unit (sub-facies 2a)

The Cyclic Varve Unit is distinguished by dark laminae forming a rhythmic facies and comprised a repetitive asymmetrical laminations of a thicker medium to dark mudstone (0.1–1 cm), in sharp contact with a thinner and well cemented very fine brown carbonate mudstone (Figure 12a), dominated by Mn carbonate (kutnohorite; 0.001–0.1 cm). The gradual increase to darker shades of grey within each of the thicker mudstone laminations suggests a gradual increase in OM content with each cycle. The kutnohorite laminae contain less OM (Figure 17a and b). Mineralogically, the Cyclic Varve Unit is very variable (Table 6), which is consistent with the

heterogeneous appearance of the sub-facies. XRD identified clays, quartz, albite, carbonates, jarosite, gypsum, and pyrite. Clay phases include illite/mica, kaolinite and, chlorite. Carbonate phases, i.e. dolomite and kutnohorite, are typically restricted to the low TOC kutnohorite laminae as indicated by EDS mineral mapping (Figure 17).

Massive Black Shale (sub-facies 2b)

This sub-facies has a less pronounced rhythmicity than Cyclic Varve Unit. The Massive Black Shale is confined to the lower 15 m of the Stuart Range Formation within Arck 1. At whole core scale, this sub-facies appears to be relatively homogenous. However, SEM-based mineral distribution mapping identifies heterogeneities and subtle laminations. It comprises approximately 10 cm thick alternating bands of lighter and darker mudstone and is interlaminated by mm-scale laminae. The darker mudstone is texturally more complex with more laminae (Figure 14b). EDS mineral mapping (Figure 15b) shows that these finer-scaled laminae comprise alternating bands of kutnohorite and gypsum with clays and quartz. In order to identify high resolution spatial patterns of mineral phases, the novel approach of EDS integrated with Quantitative Evaluation of Minerals by Scanning electron microscopy (QUEMSCAN®), was conducted on polished blocks taken from the Massive Black Shale (Figure 18). The detrital grains are comprised of poorly sorted, sub-angular to sub-rounded quartz grains (<250 µm) with occasional tabular K-feldspar (<100 µm), illite aggregates (<50 µm) and minor muscovite (<25 µm). The matrix is comprised of illite, kaolinite, chlorite (clinochlore and chamosite) and authigenic quartz (<5 µm). Abundant pyrite framboids occur only within phyllosilicate intervals, which alternate with kutnohorite dominated laminae. Mineralogically, the massive black shale was heterogeneous and similar to that of the Cyclic Varve Unit, with varying presences of chlorite and feldspar.

Lensed Mudstone (sub-facies 2c)

This sub-facies dominates the upper Stuart Range Formation in Arck 1. The Lensed Mudstone is characterised by alternating bands of dark and light mudstone, varying in thickness from millimetre- to centimetre-scales (Figure 14c). Laminae are discontinuous and typically homogenous with minimal internal gradation. Common lensoid and lenticular segregations (2–8 cm length and <2 cm width) form parallel to laminae and are comprised of subhedral calcite, and are interpreted to be cemented burrows. On the basis of the homogeneity and discontinuity of laminae, sediment reworking by bioturbation may have been prevalent during deposition. Mineralogically, the lensed mudstone is very similar to the other two sub-facies within the Pelagic

Facies (Table 6), though the Lensed Mudstone also contained K-feldspar and minor mixed layer illite–smectite.

BIOTURBATED FACIES

The bioturbated facies is a massive calcareous marl that is more pervasively laminated toward the upper boundary of the unit. Residual structures of primary lamination can be distinguished in most intervals, and rip-up clasts (0.5–2.0 cm) and soft sedimentary deformation are present along the lower boundary surface, which is often undulating and non-horizontal. Burrow shapes are commonly observed (Figure 13c), and this, together with the homogeneity of the unit and the interruption of pre-existing laminae, suggests bioturbation in oxygenated bottom water conditions. However, relics or traces of benthic organisms are absent. Mineralogy is dominated by dolomite, and contains quartz, illite/mica, kaolinite, and apatite (Table 6).

The main macerals identified by organic petrography are terrestrially-derived inertinite (semifusinite) and vitrinite (telinite). Liptinite is also present, though only minor. Distinct, tabular woody tissue (telinite) occurs as angular fragments in high abundances, and range up to 50 µm in size. The different distribution of macerals in this facies, in comparison to the Pelagic Facies, could result from different input or selective preservation resulting from the greater resistance of terrestrial OM toward oxidation (Freudenthal *et al.* 2001). Thus, the dominance of terrestrial OM in lower TOC intervals may reflect more oxic bottom water conditions and reduced liptinite (lamalginite and sporinite) OM preservation efficiency.

MASS FLOW FACIES

Total organic carbon (TOC) variations in Arck 1 are predominately distributed between the organic-lean Mass Flow Facies and organic-rich Pelagic Facies (Figure 12). The Mass Flow Facies comprises up to 60 cm thick intervals (minimum thickness observed is 2 cm) of a massive, calcareous, low TOC mudstone, occurring approximately every 10 m. Internally, it comprised minor discontinuous dark laminae that gradually became more laminated toward the top. A white lonestone (2 x 3 cm) with compaction-related sediment deflection was identified within one interval at 960.58 m in the Arck 1 core implying the continuation of ice rafting (Figure 13d). Very abrupt, erosive lower boundaries suggest rapid onset of mass deposition, suggesting a mass flow deposit. XRD identified quartz, albite, carbonates, pyrite, and minor clays (kaolinite and chlorite) in all samples analysed. Carbonate phases are dominated by dolomite, kutnohorite, and siderite.

SOURCE ROCK CHARACTERISATION

Organic carbon (OC) within the Stuart Range Formation, Arck 1, is Type II–III oil-gas-prone to Type III gas-prone as indicated by high hydrogen index (HI) values of up to 400 mg HC/g TOC TOC (Figure 20). It is marginally mature, heading into the oil generation window. Analysis by gas chromatography-mass spectrometry (GC-MS) and micro-scale-sealed-vessel thermal extraction and pyrolysis technologies hyphenated to GC-MS (MSSV-GC-MS) identifies mainly low molecular weight macromolecules, typical of light oil. Rock-Eval (SRA analysis) indicates the proportion of free hydrocarbons (S1) that evolve from a rock sample without cracking kerogen during the first stage (heating at 300 °C) of stimulated maturation. The proportion of hydrocarbons with generative potential (S2) correspond to hydrocarbons that evolve during the second stage (heating above 300 °C) of stimulated maturation. The S1 component within the Stuart Range Formation yields 0 to 0.96 mg HC/g rock and the S2 component varies between 0.53 and 33.02 mg HC/g rock (Figure 21). The maximum S2 value is very high relative to the S1 value, implying good source rock potential. However, a high S2 is unfavourable in terms of immediate oil production within the Arckaringa basin. There is significant risk that the thermal maturity of the Stuart Range Formation is not sufficient to have generated hydrocarbons across the basin. Nonetheless, these organic rich shales may also be in the oil generation window where deeper burial has already occurred or where a higher geothermal gradient is present.

The Cootanoorina Formation comprises Type IV inert to Type III gas-prone OC as indicated by HI values averaging less than 20 mg HC/g TOC, and ranging up to 100 mg HC/g TOC (Figure 20). This formation has no to very minor potential to produce hydrocarbons, and these hydrocarbons may have already matured migrated to shallower parts of the basin. Alternatively, this formation may have never had any significant potential to produce hydrocarbons. Rock-Eval indicates that the S1 yields values between 0.01 and 0.03 mg HC/g rock and that the S2 component varies between 0.02 and 0.08 mg HC/g rock (Figure 21). The Cootanoorina Formation had multiple S2 peaks, suggesting multiple stages of maturation and multiple phases of migration, potentially representing a new source of hydrocarbons for the Arckaringa hydrocarbon system, within the shallower parts of the basin. The Cootanoorina Formation hydrocarbons may be contributing to the minor oil shows in Maglia 1.

Lambina 1, to the north of the basin, does not intersect the Stuart Range Formation. Analyses were run on the Mount Toondina Formation and the Boorthanna Formation which comprise Type IV inert OC, as indicated by low HI values of 55 to 135 mg HC/g TOC. However, higher values

may indicate sediments that are gas prone at best (Figure 20). Yields of combined S1 and S2 range from 0.20 to 0.63 mg HC/g rock, indicating poor source rock quality and low potential for hydrocarbon generation (Figure 21). This is consistent with the view that the focus for future exploration should be the southern part of the basin where there is increasing thermal maturity from greater burial.

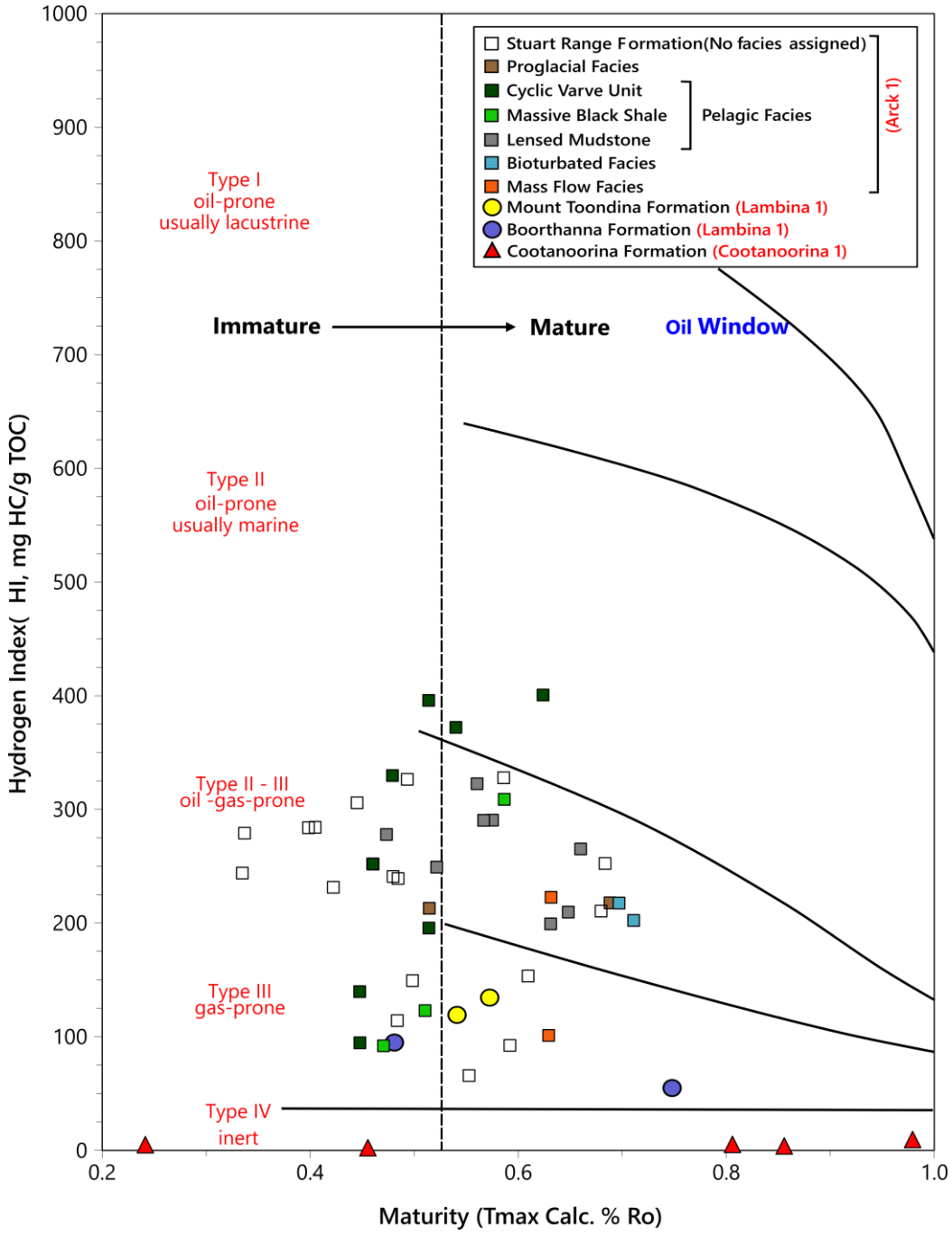

Figure 20: The types of hydrocarbons and the maturity of a selection of Arck 1, Cootanoorina 1, and Lambina 1 core samples, based on source rock analysis (SRA). The Stuart Range Formation (box), taken from the Arck 1 core, is primarily Type II–III oil-gas-prone to Type III gas-prone as indicated by the low hydrogen index (HI) values. It is immature to mature, heading into the oil generation window. The Stuart Range Formation samples have been coloured according to their facies. Samples without an assigned facies have not been coloured. The Cootanoorina Formation (red triangle), taken from the Cootanoorina 1 core, is Type IV inert to Type III gas-prone as indicated by the extremely low HI values. This formation has no potential to very minimal potential to produce hydrocarbons. From Lambina 1, the Mount Toondina Formation (yellow circles) and Boorthanna Formation (purple circles) are Type IV inert, however, higher values within the Mount Toondina Formation may be gas prone at best.

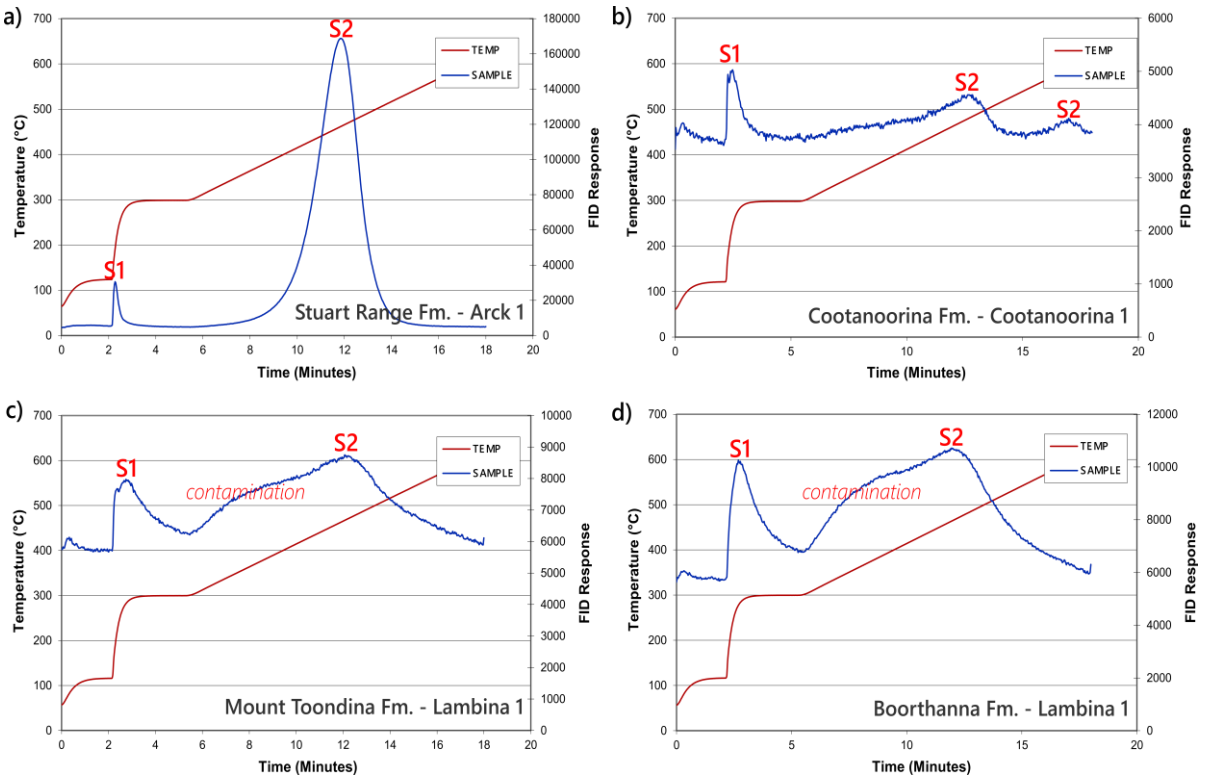

Figure 21: Representative source rock potential pyrograms based on source rock analysis (SRA). The plots show the proportions of free (S1) and potential (S2) hydrocarbons as artificial maturation is induced by incrementally increasing temperature over a period of time. (a) Stuart Range Formation (2053193, 963.04 m), from Arck 1 core, has a significant hydrocarbon potential as indicated by the large S2 peak. The comparatively low S1 peak indicates a low proportion of free hydrocarbons. (b) Cootanoorina Formation (2066664,948.06 m), from Cootanoorina 1 core, has multiple S2 peaks, suggesting multiple stages of maturation and multiple phases of migration. Both (c) Mount Toondina Formation (2131268, 411.48-414.53 m) and (d) Boorthanna Formation (2131269, 435.86-438.91 m) from Lambina 1 cuttings, indicate low yields of S1 and S2, suggesting poor source rock quality and low potential for hydrocarbon generation. Contamination due to drilling fluids are present in these cuttings.

Organic Geochemistry

Geochemical analysis of the organic compounds within OM extracted from different facies was undertaken to determine the systematic variations in primary OM input to each facies and to identify a mechanism of OM preservation. There is a systematic difference in composition of the organic-rich Pelagic Facies and the organic-lean Bioturbated Facies and Mass Flow Facies. The Pelagic Facies contains high sulphur compounds such as dibenzothiophene (DBT, *m/z* 184), methyldibenzothiophene (MDBT, *m/z* 198), and dimethyldibenzothiophene (DMDBT, *m/z* 212). These organosulphur compounds are significantly correlated with total OC content (Figure 22). Their presence coincides with high pyrite abundance within the Pelagic Facies, indicating high sulphur concentrations, and they are at a low concentration (near detection limit) within the organic-lean facies. High sulphur concentrations were also measured within lipid-rich OM in the organic-rich intervals by EDS spot analysis. This, together with the distribution of organosulphur

compounds with TOC, is consistent with sulfurization reactions leading to polymerization (Burdige 2007).

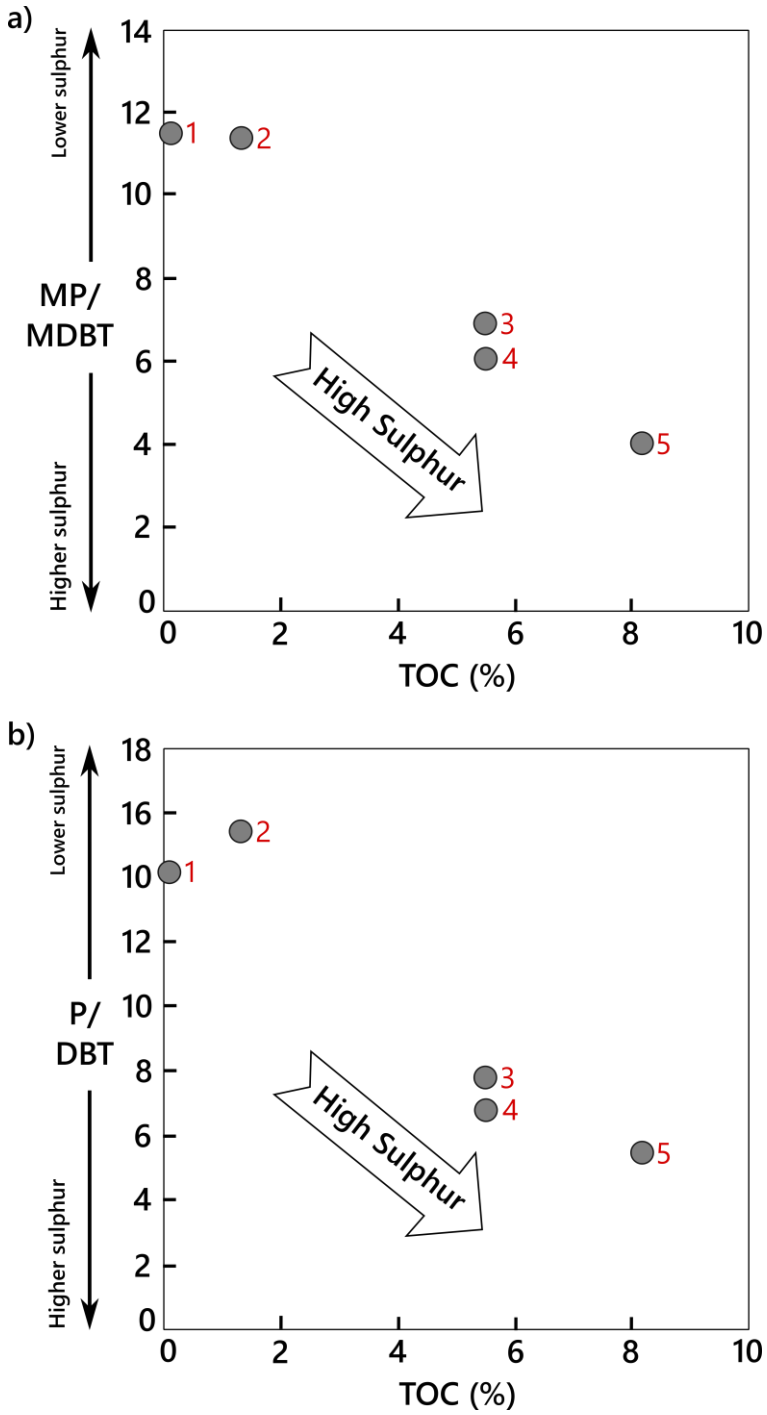

Figure 22: Organosulphur compounds significantly correlate with percentage total organic carbon (TOC %) content. Samples from the Stuart Range Formation (Arck 1) are indicated as: 1 = 2053195, 2 = 960 (x2), 3 = 960 varve, 4 = 962.54, and 5 = 2053188. (a) Methylphenanthrene/methyldibenzothiophene (MP/MDBT) against TOC, and (b) Phenanthrene/dibenzothiophene (P/DBT) against TOC, a decrease in the ratios MP/MDBT and P/DBT indicates an increase in the presence of organosulphur compounds, as shown by the arrow.

Both marine and terrestrial OM signals were identified during GC-MS analyses, consistent with organic petrography and SEM results. The Bioturbated Facies and Mass Flow Facies (samples 1 and 2 respectively) show terrestrial affinities, with greater C_{29} sterane abundance, and are likely to be more gas prone than the Pelagic Facies (samples 3, 4, and 5) which shows marine (algal) affinities with slightly less C_{29} steranes (Figure 23). The Pelagic Facies comprise abundant C_{30} 4-desmethylsteranes, a reliable source parameter for identifying marine algal OM input that is oil prone (Peters and Moldowan 1993). A larger marine algal-bacterial OM contribution within the Pelagic Facies is also suggested by the predominance of C_{23} tricyclic terpanes over C_{24} tetracyclic terpanes (Figure 24). C_{24} tetracyclic is considered to be a terrestrial indicator (Philp and Gilbert 1986), and the ratio of C_{24}/C_{23} is low (0.30 – 0.45) in the organic-rich Pelagic Facies and high (0.50 – 0.63) in the organic-lean Bioturbated Facies and Mass Flow Facies. Consistent with the algal OM identified within organic-rich intervals from organic petrography, there is a dominance of marine-derived compounds in organic-rich intervals, suggesting greater oil production potential. Likewise, the dominance of terrigenous compounds the organic-lean intervals could result from different input or preservation resulting from the greater resistance of terrestrial OM toward oxidation (Freudenthal *et al.* 2001).

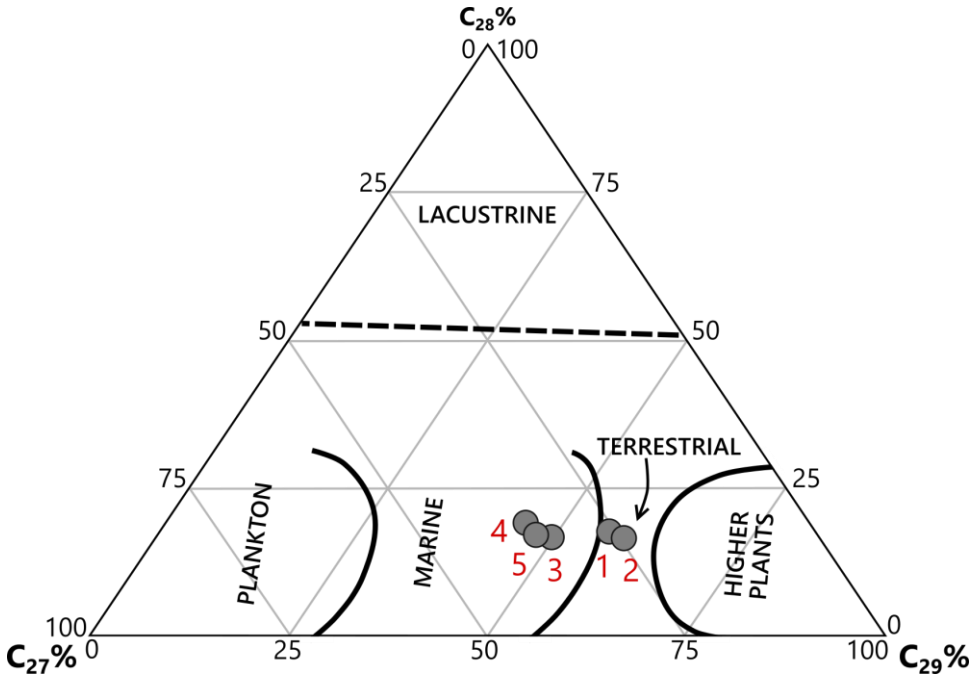

Figure 23: Ternary diagram of C_{27}, C_{28}, and C_{29} ααα R sterane proportions (%) of the Stuart Range Formation using organic carbon source fields defined by Huang and Meinschein (1979). Samples are indicated as: 1 = 2053195, 2 = 960 (x2), 3 = 960 varve, 4 = 962.54, and 5 = 2053188. The high concentrations of C_{27} and C_{29} steranes reflect typical Palaeozoic marine biota and terrestrial input. The organic-lean intervals (samples 1 and 2) are characteristically terrestrial with greater C_{29} steranes, whereas the organic-rich intervals (samples 3, 4, and 5) are characteristically marine (algal) with slightly less C_{29} steranes.

Reactive compounds are more abundant in the Pelagic Facies, such as 1,8-DMN, 1,5-DMN and 1,4-DMN αα- isomers and hopenes. These compounds are thermodynamically unstable and prone to degradation (Ten Haven *et al.* 1986; Budzinski *et al.* 1993). A preservational mechanism is required to stabilise these compounds and account for the high concentrations of organosulphur compounds within the organic-rich intervals, and polymerization from sulfurization reactions is a potential mechanism for this.

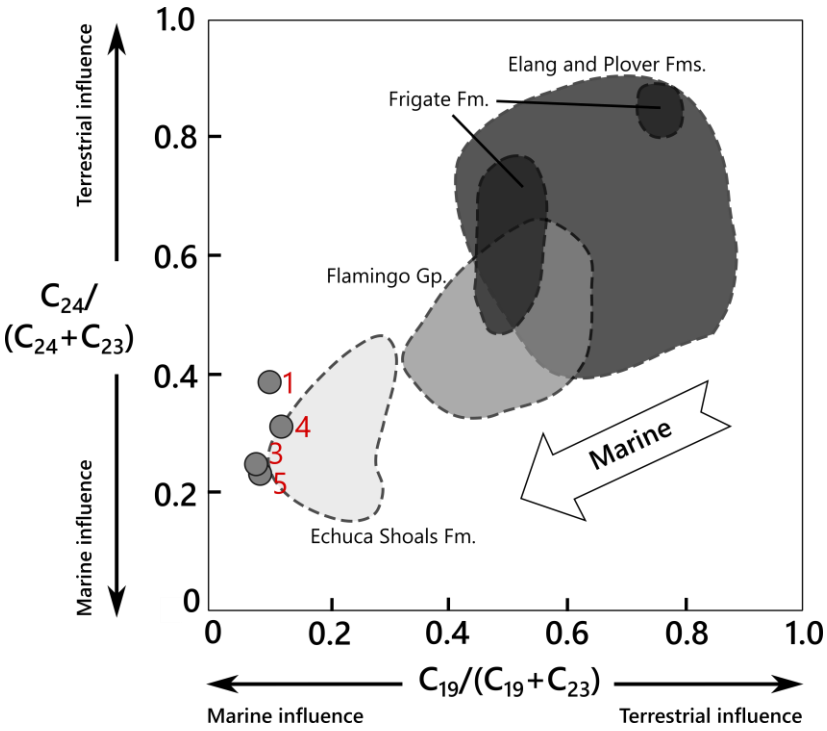

Figure 24: A plot of C_{24} tetracyclic terpanes/(C_{24} tetracyclic terpanes+C_{23} tricyclic terpanes) against C_{19} tricyclic terpanes/(C_{19} tricyclic terpanes+ C_{23} tricyclic terpanes), calculated from the *m/z* 191 chromatograms. The ratios for the Stuart Range Formation has been plotted here, showing the dominance of marine input as indicated by the arrows. As the ratios decrease there is an increase in marine influence. Samples are indicated as: 1 = 2053195, 3 = 960 varve, 4 = 962.54, and 5 = 2053188. Sample 1 (Bioturbated Facies) shows a greater terrestrial influence, consistent with Figure 23. Sample 960 (x2) was not plotted as C_{19} was not identified within this sample. The grey fields are taken from prior studies on oils from the Jurassic-Cretaceous Bonaparte Basin for comparison, after Preston and Edwards (2000).

DISCUSSION

Organic carbon enrichment in the Stuart Range Formation is unusual due to its cold-climate palaeoenvironment, form of organic matter particles, mm-scale alternation of early diagenetic phases, and chemically immature, feldspathic mineralogy. This thesis tests the hypothesis that episodic restriction of fault bounded and glacially scoured troughs within the basin facilitated oscillating water column redox conditions, favouring sulfurization reactions and leading to

preservation in organic-rich varves. To test this hypothesis geographical, sedimentological, mineralogical, and geochemical evidence was collected to determine the timing, composition, and variation of organic-rich laminae and organic-lean laminae.

The Arckaringa Basin sediments were deposited during the waning stages of the Permo-Carboniferous ice age in Australia. A change from tropical equatorial carbonitic and evaporitic conditions to high-latitude glacial conditions occurred in the Carboniferous with Gondwana's southward progression (Veevers 2006). A combination of latitudinal changes and highland development resulted in continental style glaciation beginning in the mid-Carboniferous, evidenced by striated and fluted cobbles, and glendonites (Wopfner 1970; Crowell and Frakes 1971). Active glaciation is also suggested by the U shaped morphology of the troughs in seismic profiles, and the presence of rainout clastic material and dropstones within the Proglacial Facies of the Boorthanna Formation. A dominance of physical over chemical weathering typical of glacial conditions is indicated by the abundance of feldspar silt grains indicating a mineralogical immaturity of the sediments, which are angular and poorly sorted indicating limited physical transport. The great majority of organic-rich sediments in the geological record are associated with greenhouse conditions (Klemme and Ulmishek 1991; Weissert and Mohr 1996), the cold climate conditions prevalent during deposition of the Boorthanna and Stuart Range Formations are not commonly associated with organic carbon (OC) enrichment. Though equivalent source rocks in the Cooper Basin, 350 km north-east of the Arckaringa Basin, were deposited at similar latitudes and under glacial conditions, the Arckaringa Basin shows unique mineralogy and geochemistry. The isolated connection of the Arckaringa Basin to the open ocean is responsible for these differences.

Though most glaciers were sourced from Antarctica, local glaciers from highlands, such as the Peake and Denison Ranges adjacent to the Boorthanna Trough, are thought to have formed the troughs due to the orientation of the troughs (east to west) and the composition of erratics and dropstones (composition of the Peake and Denison Ranges rocks). These glaciers may have moved across the basin and scoured the topography (Ludbrook 1967; Wopfner 1980; Menpes *et al.* 2010b). The evidence for glaciation, as well as steep walls and great depths, indicates that a combination of ice loading and glacial scour contributed to the morphology of these troughs, with subsequent extensional faulting observed in the seismic profiles (Figures 8 and 9). The U-shaped morphology and absence of bounding faults of the Wallira Trough is particularly consistent with a fjord interpretation. Accumulation of sediments in the troughs increased crustal

loading and caused the syn-sedimentary subsidence evident in seismic surveys (Figure 9). The deep, narrow, fjord-shaped troughs (Figure 8 and 9) would have been prone to restriction, given that exchange with the open ocean is commonly restricted in glacially scoured valleys by the presence of terminal end-moraines acting as a sill (Howe *et al.* 2010). The Stuart Range Formation was deposited in this restricted system during a deglaciation transition period.

Millimetre-scale cyclic variations in mineralogy and total organic carbon (TOC) occurring within the Pelagic Facies are similar to varved deposits associated with restricted bodies of water in paraglacial settings where strong seasonal changes in discharge and turn over influence sediment composition (Stickley *et al.* 2005). These types of deposits are also common in fjords with marine restrictions from end moraines which act as sills limiting seawater influx. The presence of sills acts to modify water chemistry in the fjord in response to changes in sea level. The oscillation between organic-rich laminae and organic-lean, carbonate laminae describes a repetitive process that is constrained by the timing of the cyclicity acting on the system. In many marine systems, such as the modern restricted basins of east Antarctica (Stickley *et al.* 2005), varves are considered to record seasonal stratification at annual time scales as well as storm disturbances (2–30 years), climate trends (100–300 years), and Milankovitch forcing (19,000 year precession or 41,000 year obliquity periodity; Anderson 1964; Peizhen *et al.* 2001). Although it cannot be determined if the varved sequences within the Arckaringa Basin are seasonal, it is apparent, based on the thin laminae (0.001 to 1 cm), that cyclical processes are acting on short timescales within the system and it is reasonable to suggest seasonality.

This study addresses the mechanisms of OC preservation in the absence of the influences typical of source rocks forming in greenhouse conditions, such as preservation through association with detrital clay minerals. Clay mineral surfaces stabilise otherwise labile organic compounds, contributing to the organic enrichment of typical, greenhouse source rocks (Keil *et al.* 1994; Kennedy and Wagner 2011). The cold-climate organic-rich Stuart Range Formation, however, is an immature feldspathic micaceous siltstone. This reflects the dominance of physical over chemical weathering, so that high surface area clay minerals typically formed in soils are not significant and thus cannot account for OC preservation in the same way as the class of source rocks deposited during greenhouse conditions. Petrographic analysis shows that OM occurs as micron-scale, discrete particles (Figure 11), rather than as organo-clay aggregates.

High resolution mineral and elemental mapping and spot analysis within the Pelagic Facies in the Stuart Range Formation reveals systematic variations in elemental and mineral distributions. Manganese (Mn) and sulphur (S) enrichment are of particular interest and are associated with mm-scale couplets, where kutnohorite (Mn carbonate) laminae alternate with S-enriched OM-rich, pyritic laminae. For instance, within the Pelagic Facies, dark laminations compared to light laminations have higher TOC content. Also coincident with the darker mudstone laminations is an abundance of framboidal pyrite of up to 20%. Framboidal pyrite formation is commonly interpreted as the product of bacterial reduction of seawater-derived sulphate, which forms hydrogen sulphide (H_2S) and reacts with dissolved iron to form pyrite (Berner 1982). Pyrite can only form in the absence of oxygen and the presence of H_2S, and these conditions identify euxinia. As H_2S is only available under euxinic conditions, this indicates bottom water or water column euxinia at the time dark laminae were deposited. The abundance of framboidal pyrite, the S enrichment in OM (lamalginite and sporinite), and the abundance of organosulphur compounds within organic-rich intervals further indicate euxinia during sediment deposition and early diagenesis. On the other hand, the paler kutnohorite laminations that alternate with the darker laminations identify oxygenated conditions (Huckriede and Meischner 1996).

The abundance of sulphides within organic-rich laminae is consistent with the hypothesis that sulfurization led to preservation. Sulphate is one of the dominant anions in sea water, but is present only at very low concentration in almost all lacustrine systems. A high abundance of sulphides (S) thus suggests a sea water source for S found in the abundant framboidal pyrite. This in turn implies a marine connection facilitating S resupply. The abundance of framboidal pyrite within the Pelagic Facies identifies sulphate reduction, which is energetically favoured only after free oxygen is no longer available as an oxidant. The development of seasonal strong density stratification, resulting in the development of anoxia, can be achieved through various mechanisms. Warmer surface waters with a freshwater influx and lower density will cap cooler, saline waters, leading to density stratification. The Baltic Sea is one example of this (Emeis *et al.* 2003). However, katabatic winds together with frequent thermal inversions during cooler seasons will lead to well mixed and oxygenated waters. Restriction of marine in flow and bottom-water exchange, by a sill for example, leading to density stratification commonly results in anoxic conditions and H_2S build up in modern examples such as the Framvaren Fjord in Norway (Saelen *et al.* 1993; Meyer and Kump 2008), the Skagerrak Fjord in Germany (Aure *et al.* 1996), the Ellis Fjord in eastern Antarctica, the Baltic Sea in central Europe (Huckriede and Meischner 1996) and the Black Sea in southeast Europe (Murray *et al.* 2007). Examples also include ancient analogues,

such as the Karoo Basin in South Africa (Haldorsen *et al.* 2001; Maruoka *et al.* 2003) and the East Greenland Basin in Greenland (Piasecki and Stemmerik 1991). These are restricted from the open ocean by a sill or landmass, and are characterised by strong density stratification and S-rich euxinic conditions with high TOC values within sediment. Within the Stuart Range Formation, particularly within the lower 15 m of the formation where the Massive Black Shale and Cyclic Varve Unit dominate, geochemical evidence and pyrite abundance supports the hypothesis of systematic development of euxinia with a build-up of H_2S (Figure 25). The reducing conditions would have provided a chemical trap for S, expressed as the observed abundance of pyrite framboids and organosulphur compounds.

Enhanced water exchange with open ocean waters or flushing of stratified waters can occur periodically or aperiodically, depending on factors such as tide, season, fresh water input, and seasonal heating (c.f. Howe *et al.* 2010). This exchange re-oxygenates the bottom waters, resulting in a downward shift of the pycnocline to interstitial waters a few centimetres below the sediment–water interface (Meyer and Kump 2008; Howe *et al.* 2010). Changes in oxygenation in the benthic environment are recorded by intermittent intervals of bioturbation in the Bioturbated Facies (Figure 13). Bioturbation causes mixing, homogenisation and irrigation, allowing oxygenated water to penetrate the sediment (Aller 1984). This can impede OM preservation by remineralising OM at a more rapid rate (Aller 1994; Hartnett *et al.* 1998).

Manganese has a short oceanic residence time (5–25 years) and therefore the fate of Mn is largely dependent on the capture and stabilisation of Mn in marine sediments (Klinkhammer and Bender 1980; Burke and Kemp 2002). The kutnohorite laminations that alternate with the darker laminations in the Pelagic Facies within the Stuart Range Formation are similar to those described from modern sediments in the anoxic Baltic Sea (Huckriede and Meischner 1996), which contain high concentrations of dissolved Mn, but experience seasonal oxygenation resulting in the oxidation of manganese (Mn^{2+}) to fine-grained particulate oxides. With a return of anoxic conditions, manganese oxides dissolve and Mn^{2+} accumulates in shallow sediment. Bacterial sulphate reduction of OM results in highly alkaline conditions (Figure 25). High alkalinity in the presence of Mn^{2+} liberated from manganese oxides leads to the precipitation of kutnohorite above the anoxic sediments in the Baltic (Huckriede and Meischner 1996). Kutnohorite laminae form on seasonal timescales as varves (Burke and Kemp 2002), related to late winter–spring flooding events. By analogy, the rapid alteration between pyritic organic-rich laminae and kutnohorite laminae suggests seasonal oscillation in benthic redox conditions in the Pelagic

Facies. This requires a physical barrier, such as a sill suggested by the basin trough morphology in seismic profiles, which would enhance sensitivity to changes in sea level and climate. Sea level fluctuations influence the magnitude of bottom water exchange over time, as recorded in the Pelagic Facies, and may consequently explain the variation in the types of OM preserved.

Sulfurization reactions (also known as vulcanization) result in the enrichment of S in OM and involve the incorporation of inorganic S into lipids and carbohydrates to form organosulphur compounds during early diagenesis (Burdige 2007). Microbial sulphate reduction during early sediment burial, $2CH_2O + SO_4^{2-} \rightarrow 2HCO_3^- + H_2S$, results in H_2S build up below the pycnocline, leading to water column formation of pyrite in small (10 µm) framboids and the incorporation of S into OM. Sulfurization has been shown to increase carbon preservation in recent sediments (Wakeham *et al.* 1995; Adam *et al.* 1998 and references therein). A study by Tegelaar *et al.* (1989) indicates that, in certain environments, these reactions can facilitate the preservation of structural information in reactive biomarkers, by preventing the degradation and remineralisation of sulphurised biolipids. Studies on the Karoo Basin (Maruoka *et al.* 2003), East Greenland Basin (Piasecki and Stemmerik 1991; Syvitski *et al.* 1996), Ellis Fjord (Sinninghe Damsté *et al.* 2007), and Black Sea sediments (Wakeham *et al.* 1995) show incorporation of reduced inorganic S in OM as a result of sulfurization during early diagenesis. The former three settings are of particular relevance to the Arckaringa Basin as these are associated with glacial, cold climate conditions within restricted marine environments.

Organic-rich laminae in the Stuart Range Formation contain particulate algal OM that is distinct from the refractory and more resistent OM observed in the organic-lean laminae. Organic geochemistry indicates that these particles are hydrogen rich and labile. Reactive compounds, such as 1,8-DMN, 1,5-DMN and 1,4-DMN αα- isomers and hopenes, are more abundant in the Pelagic Facies. Stabilisation of labile organic material by sulfurization is further suggested by the high abundance of sulphur compounds and the strong positive correlation between organosulphur compounds and TOC in the Pelagic Facies (Figure 22). It is envisaged that sulfurization was influenced cyclically by sea level change or seasonal overturning, which enhances or restricts water exchange across a sill at the head of the troughs, influences the depth of the pycnocline and influences the efficiency of sulphur bonding as a preservational mechanism (Figure 25). In the Stuart Range Formation, unlike the labile sporinite and algal macerals with incorporated S, the refractory terrestrially-derived OM is not sulfurized. When the system does not have the capacity for sulfurization through development of a euxinic water column, the

sporinite and algal macerals show limited preservation potential. The formation of pyrite is a kinetically favoured process over the formation of organosulphur compounds (Sinninghe Damste and De Leeuw 1990), and thus there must have been a limited availability of reactive Fe^{+2} to allow these reactions to occur. Seasonal variation of organic input may have also influenced the degree of OC enrichment and extent of sulfurization reactions.

Equivalent strata (Roseneath, Murteree, and Epsilon Formations) in the Cooper Basin source rocks, 350 km north-east of the Arckaringa Basin, comprise a feldspathic immature mineralogy, similar thermal maturities, and were deposited at equivalent latitudes during the waning stages of the Pennsylvanian to early Permian glaciation (Hill et al. 2011). However, were deposited under freshwater lacustrine conditions rather than marine, and thus rather than a dominance of Fe sulphides (pyrite) as observed in the Arckaringa Basin, there is a dominance of Fe-rich siderite cement, indicating S limitation (Rezaee and Schulz-Rojahn 1998). While similar physical conditions governed deposition of sediment in the Cooper Basin during this time, OM has a low hydrogen index even though sedimentological studies indicate anoxia also occurred during deposition. OM consequently has very low hydrocarbon generation potential relative to the Arckaringa Basin, even though similar TOC values are recorded (Granger 2013). The lack of a sea water connection for resupply of S likely made OM more reactive without the sulfurization reactions common in the Arckaringa Basin.

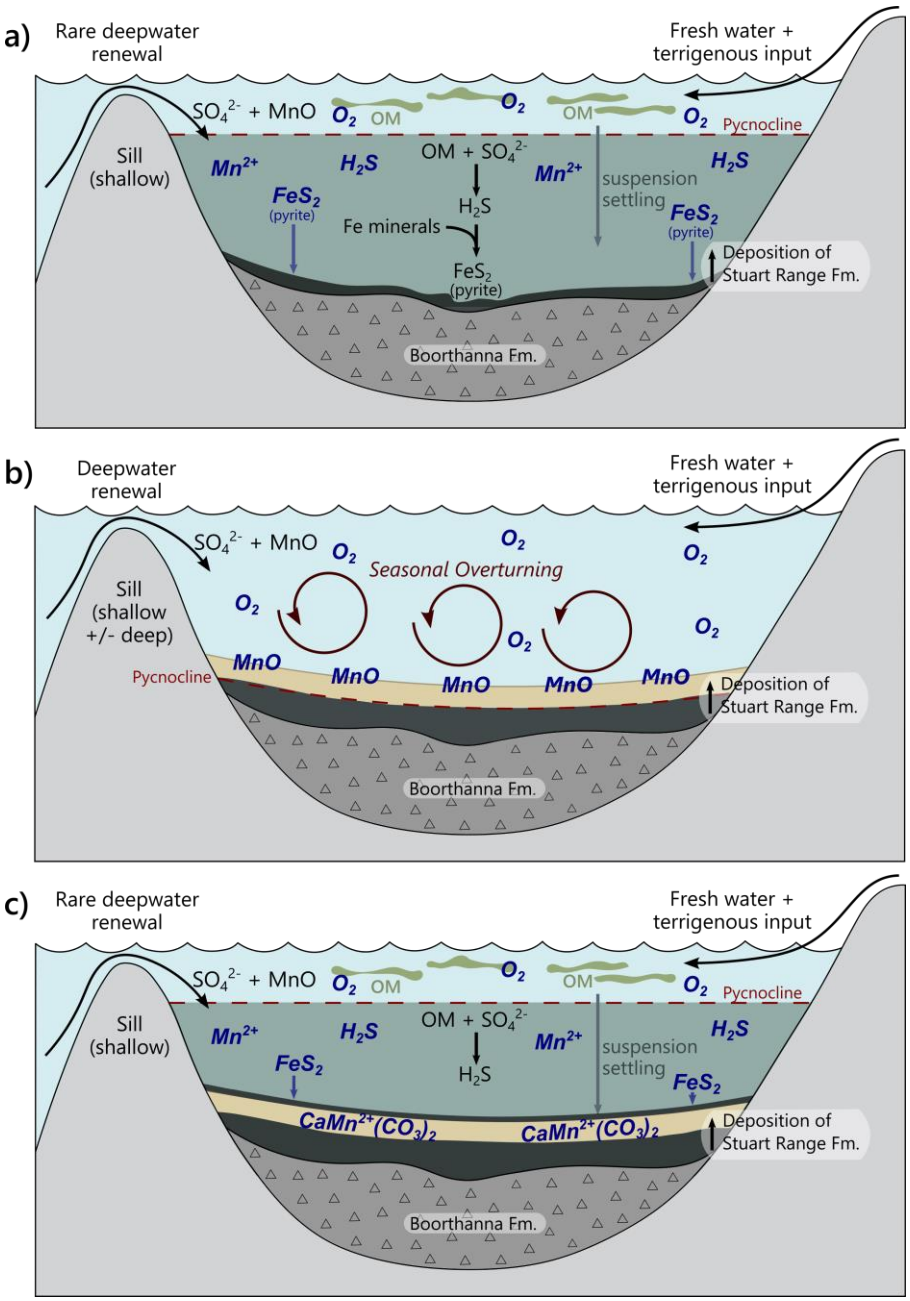

Figure 25: Schematic diagram illustrating changes in bottom water redox conditions. Connection with the open ocean water across the sill allows sulphate (SO_4^{2-}) replenishment. This diagram also shows the fluxes of fresh water, terrigenous material, and organic matter (OM) during deposition of the Stuart Range Formation. (a) Shallow sill euxinic conditions. Rare deep water renewal and a shallow pycnocline, promotes the development of stratified, euxinic bottom water conditions. The sulphur cycle, occurring within the euxinic zone, shows the partial removal of SO_4^{2-} by bacterial sulphate reduction to make sulphide or hydrogen sulphide (H_2S). H_2S can then react with the iron (Fe) minerals within the water column or sediments to precipitate pyrite (FeS_2). Fine-grained sediments are deposited as laminations in this undisturbed setting. (b) Shallow (± deep) sill oxic conditions. Frequent deep water renewal and a pycnocline within the interstitial waters a few centimetres below the sediment–water interface. Mixing of the water column with oxygen and nutrients promotes benthic fauna activity within the oxic sediments (bioturbation). Particulate manganese oxides (MnO) at sediment-water interface. (c) Reducing conditions re-establish as oxygen becomes depleted. Alkalinity from bacterial sulphate reduction and dissolution of MnO re-precipitates Mn for final transformation into kutnohorite ($CaMn^{2+}(CO_3)_2$). This model primarily applies to the lower Stuart Range Formation where pelagic settling of the Massive Black Shale and Cyclic Varve Unit dominated.

CONCLUSIONS

Seismic profiles reveal the U shaped morphology of basin troughs formed due to glacier scour and successive extensional faulting. Within these fjord-shaped troughs, restriction likely resulted from terminal moraines at the head of the fjords acting as sills to the open ocean. The Stuart Range Formation was deposited in this episodically restricted system during a deglaciation transition period. In drill core the Proglacial Facies, confined to the basal 12 m of this formation, is transitional with the underlying Boorthanna Formation.

The immature feldspathic micaceous composition of the Stuart Range Formation reflects a dominance of physical weathering typical of icehouse environments where chemical weathering is limited. This mineralogy is not characteristic of typical source rocks which are often dominated by detrital clay minerals formed in temperate to subtropical soils. Framboidal pyrite (<5 μm) is abundant and comprises up to 20% of the organic-rich intervals. This sheds light on the peculiarity of the arkosic mineralogy of Stuart Range Formation siltstones, whose presence and distribution, at fine resolutions, was made available by EDS mineral mapping. Organic carbon (OC) is dominated by discrete particles of organic matter (OM) in contrast to organo-clay aggregates common in many source rocks. OM particles are predominately hydrogen-rich and labile, rather than refractory terrigenous material, thus identifying an active preservational mechanism that differs from conventional organic carbon enrichment controlled by mineral preservation effects.

Within the Pelagic Facies, sulphur/organic-rich laminae and organic-lean laminae featuring manganese carbonate (kutnohorite) cyclically alternate at millimetre scales. This identifies oscillating benthic redox conditions similar to couplets comprising annual varves in proglacial environments. OC enrichment is attributed to restriction in the troughs, leading to periods of hydrogen sulphide build up within the water column. Reducing conditions provided a chemical trap for sulphur leading to its enrichment in pyrite and OM within the organic-rich intervals. Framboidal pyrite is abundant only within organic-rich laminae, indicating sulphate reduction in euxinic conditions resulting from restricted sea water exchange and the development of strong density stratification. The abundance of organosulphur compounds within the organic-rich laminae is consistent with sulfurization reactions leading to polymerization and preservation of labile organic compounds (lipids and carbohydrates) during early diagenesis. Episodic oxygenation of bottom waters oxidised Mn^{2+} to particulate oxides at the sediment-water interface. As the reducing conditions re-established, the alkalinity produced from bacterial

sulphate reduction of OM re-precipitated manganese for final transformation into manganese carbonate (kutnohorite). OM in kutnohorite laminae is mainly refractory terrigenous OC, consistent with limited preservation of labile marine OM due to improved bottom-water ventilation. Thus, sulfurization reactions were critical for OC preservation and were facilitated by restriction in the ancient fjord-like troughs. This system provides an interesting contrast to the adjacent and contemporaneous Cooper Basin which was isolated from marine waters and thus S limited. Diagenetic cements in the Cooper are Fe rich siderite. OM is refractory and particulate, of lower source quality and lacking S bonds to preserve labile OM.

ACKNOWLEDGMENTS

I am extremely grateful to my Primary Supervisor, Professor Martin Kennedy, for his invaluable wealth of knowledge and for his keen interest in developing my research and analytical skills. I am also very thankful to my Co-Supervisor, Dr Stefan Löhr, for providing constructive thesis support, valuable academic feedback and advice, and imparting his technical expertise. I also thank Professor Simon George and Dr Tony Hall for laboratory management and providing me with the opportunity to develop my technical and analytical skills. Sample preparation and experimental assistance was made possible through the help of laboratory assistants, Sarah Houlahan and Robyn Williamson. I offer many thanks to Sandy Menpes from Santos Ltd. for her ongoing advice, seismic work, and figures. Constructive feedback and project ideas developed from discussions with research colleagues, the Master of Research cohort and advisors, and James Hall are also greatly appreciated.

REFERENCES

ADAM, P., PHILIPPE, E., and ALBRECHT, P. 1998. Photochemical Sulfurization of Sedimentary Organic Matter: A Widespread Process Occurring at Early Diagenesis in Natural Environments? Geochimica et Cosmochimica Acta **62**, 265-271. doi: 10.1016/S0016-7037(97)00332-3.

ALEXANDER, E. M., GRAVESTOCK, D. I., CUBITT, C., and CHANEY, A. 1998 Lithostratigraphy and environments of deposition. In Gravestock, D. I., Hibburt, J. E., and Drexel, J. F. ed.^eds. The petroleum geology of South Australia. Vol. 4: Cooper Basin. ed. Department of Primary Industries and Resources. Report Book 98/9, South Australia.

ALEXANDRE, J. T., VAN GILST, R. I., RODRÍGUEZ-LÓPEZ, J. P., and DE BOER, P. L. 2011. The sedimentary expression of oceanic anoxic event 1b in the North Atlantic. Sedimentology **58**, 1217-1246. doi: 10.1111/j.1365-3091.2010.01202.x.

ALLCHURCH, P. D., WOPFNER, H., HARRIS, W. K., and MCGOWRAN, B. 1973 Cootanoorina No. 1 Well. In ed.^eds. pp. 1-86. ed.: Department of Mines, Geological Survey of South Australia.

ALLER, R. C. 1984. The importance of relict burrow structures and burrow irrigation in controlling sedimentary solute distributions. Geochimica et Cosmochimica Acta **48**, 1929-1934. doi: 10.1016/0016-7037(84)90375-2.

ALLER, R. C. 1994. Bioturbation and remineralization of sedimentary organic matter: effects of redox oscillation. Chemical Geology **114**, 331-345. doi: 10.1016/0009-2541(94)90062-0.

ANDERSON, R. Y. 1964. Varve calibration of stratification. In Merriam, D. G. ed.^eds. In Symposium on Cyclic Sedimentation. Kansas Geological Survey Bulletin, 1-20.

APLIN, A. C., and MACQUAKER, J. H. S. 2011. Mudstone diversity: Origin and implications for source, seal, and reservoir properties in petroleum systems. The American Association of Petroleum Geologists Bulletin **95**, 2031-2059. doi: 10.1306/03281110162.

AURE, J., DANIELSSEN, D., and SÆTRE, R. 1996. Assessment of eutrophication in Skagerrak coastal waters using oxygen consumption in fjordic basins. ICES Journal of Marine Science **53**, 589-595. doi.

BASTOW, T. P., VAN AARSSEN, B. G. K., and LANG, D. 2007. Rapid small-scale separation of saturate, aromatic and polar components in petroleum. Organic Geochemistry **38**, 1235-1250. doi: 10.1016/j.orggeochem.2007.03.004.

BERNER, R. A. 1982. Burial of organic carbon and pyrite sulfur in the modern ocean: Its geochemical and environmental significance. American Journal of Science **282**, 451-473. doi.

BUDZINSKI, H., GARRIGUES, P., RADKE, M., CONNAN, J., RAYEZ, J. C., and RAYEZ, M. T. 1993. Use of molecular modeling as a tool to evaluate thermodynamic stability of alkylated polycyclic aromatic hydrocarbons. Energy & Fuels **7**, 505-511. doi: 10.1021/ef00040a011.

BURDIGE, D. J. 2007. Preservation of organic matter in marine sediments: controls, mechanisms, and an imbalance in sediment organic carbon budgets. Chemical Reviews **107**, 467-485. doi.

BURKE, I. T., and KEMP, A. E. S. 2002. Microfabric analysis of Mn-carbonate laminae deposition and Mn-sulfide formation in the Gotland Deep, Baltic Sea. Geochimica et Cosmochimica Acta, 1589-1600. doi.

CROWELL, J. C., and FRAKES, L. A. 1971. Late Paleozoic glaciation: Part IV, Australia. Geological Society of America Bulletin **82**, 2515-2540. doi.

EMEIS, K.-C., STRUCK, U., BLANZ, T., KOHLY, A., and VOB, M. 2003. Salinity changes in the central Baltic Sea (NW Europe) over the last 10000 years. The Holocene **13**, 411-421. doi: 10.1191/0959683603hl634rp.

ESPITALIÉ, J., MADEC, M., TISSOT, B., MENNING, J., and LEPLAT, P. 1977. Source rock characterization method for petroleum exploration. Offshore Technology Conference, Houston, Texas. pp.

FREUDENTHAL, T., WAGNER, T., WENZHÖFER, F., ZABEL, M., and WEFER, G. 2001. Early diagenesis of organic matter from sediments of the eastern subtropical Atlantic: evidence from stable nitrogen and carbon isotopes. Geochimica et Cosmochimica Acta **65**, 1795-1808. doi: 10.1016/S0016-7037(01)00554-3.

GLEADOW, A. J. W., KOHN, B. P., BROWN, R. W., O'SULLIVAN, P. B., and RAZA, A. 2002. Fission track thermotectonic imaging of the Australian continent. Tectonophysics **349**, 5-21. doi: 10.1016/S0040-1951(02)00043-4.

GLEN, R. A. 2005. The Tasmanides of eastern Australia. The Geological Society of London, Special Publications **246**, 23-96. doi: 10.1144/GSL.SP.2005.246.01.02.

GRANGER, T. 2013. Mechanisms for anomalous organic matter concentrations within the Roseneath-Epsilon-Murteree section of the Cooper Basin. Honours Thesis. The University of Adelaide, Adelaide (unpubl.).

HALDORSEN, S., VON BRUNN, V., MAUD, R., and TRUTER, E. D. 2001. A Weichselian deglaciation model applied to the Early Permian glaciation in the northeast Karoo Basin, South Africa. Journal of Quaternary Science **16**, 583-593. doi: 10.1002/jqs.637.

HALL, J. W. 2014. Exhumation of the Peake and Denison Ranges; insights from low-temperature thermochronology. The Univeristy of Adelaide Adelaide (unpubl.).

HARRIS, W. K., and MCGOWRAN, B. 1968. S.A.G. Cootanoorina No. 1 Well. Upper Paleozoic and Lower Cretaceous Micropalaeontology. Grid G/3. Report 66/33. Department of Mines. South Australia.

HARTNETT, H. E., KEIL, R. G., HEDGES, J. I., and DEVOL, A. H. 1998. Influence of oxygen exposure time on organic carbon preservation in continental margin sediments. Nature **391**, 572-574. doi: 10.1038/35351.

HARVEY, S. C., and HIBBURT, J. E. 1999. Petroleum exploration and development in South Australia. 12th edition. Report Book 99/3. Department of Primary Industries and Resources. South Australia.

HAWKES, S. 2014. Arck-1 Palynostratigraphical Analysis. Palynology Report No. 2014/07. Santos Ltd. Subsurface Services Department. Adelaide.

HIBBURT, J. E. 1984. Review of exploration activity in the Arckaringa Basin region 1858 to 1983. Report Book 84/1. Department of Mines and Energy. South Australia.

HIBBURT, J. E. 1995 Arckaringa Basin. In Drexel, J. F., and Preiss, W. V. ed.^eds. The geology of South Australia. Vol. 2, The Phanerozoic. ed. South Australia. Geological Survey. Bulletin, 54, pp. 73-76.

HILL, A., MENPES, S., BACKE, G., KHAIR, H., and SIASITORBATY, A. 2011. Shale gas prospectivity in South Australia. APPEA Journal **51**. doi.

HOWE, J. A., AUSTIN, W. E. N., FORWICK, M., PAETZEL, M., HARLAND, R., and CAGE, A. G. 2010. Fjord systems and archives: a review. The Geological Society of London, Special Publications **344**, 5-15. doi: 10.1144/sp344.2.

HUANG, W.-Y., and MEINSCHEIN, W. G. 1979. Sterols as ecological indicators. Geochimica et Cosmochimica Acta **43**, 739-745. doi: 10.1016/0016-7037(79)90257-6.

HUCKRIEDE, H., and MEISCHNER, D. 1996. Origin and environment of manganese-rich sediments within black-shale basins. Geochimica et Cosmochimica Acta **60**, 1399-1413. doi.

HUNT, J. M. 1996. Petroleum Geochemistry and Geology. 2 ed. Freeman, New York.

JARVIE, D. M., CLAXTON, B. L., HENK, F., and BREYER, J. T. 2001. Oil and shale gas from the Barnett Shale, Fort Worth Basin, Texas. AAPG Annual Meeting, Denver, CO. pp. A100.

JENSEN-SCHMIDT, B., ALEXANDER, E. M., and COTTON, T. B. 2006 Structural and tectonic setting. In Cotton, T. B., Scardigno, M. F., and Hibburt, J. E. ed.^eds. The petroleum geology of South Australia, Volume 2: Eromanga Basin. 2 ed. Department of Primary Industries and Resources, South Australia., pp. 1-27.

JONES, M. J. 1987. Review of palynology, Arckaringa Basin (Newmont NB/SR 12, Birribiana No. 1 and Hanns Knob No. 1). Report 542/1. Dehli Petroleum Pty Ltd. South Australia.

JONES, P. J. 1988. Evidence for diapirism in the Arckaringa Basin, South Australia. Honours Thesis. The University of Adelaide, Adelaide (unpubl.).

KEIL, R. G., MONTLUCON, D. B., PRAHL, F. G., and HEDGES, J. I. 1994. Sorptive preservation of labile organic matter in marine sediments. Nature **370**, 549-552. doi.

KELLETT, J., VEITCH, S., MCNAUGHT, I., and VAN DER VOORT, A. 1999. Hydrogeological Assessment of a Region in Central Northern South Australia. Bureau of Rural Sciences Australia. Canberra.

KENNEDY, M. J., and WAGNER, T. 2011. Clay mineral continental amplifier for marine carbon sequestration in a greenhouse ocean. Proceedings of the National Academy of Sciences **108**, 9776-9781. doi: 10.1073/pnas.1018670108.

KLEMME, H., and ULMISHEK, G. F. 1991. Effective petroleum source rocks of the world: stratigraphic distribution and controlling depositional factors (1). The American Association of Petroleum Geologists Bulletin **75**, 1809-1851. doi.

KLINKHAMMER, G. P., and BENDER, M. L. 1980. The distribution of manganese in the Pacific Ocean. Earth and Planetary Science Letters **46**, 361-384. doi: 10.1016/0012-821X(80)90051-5.

KOHN, B. P., GLEADOW, A. J. W., BROWN, R. W., GALLAGHER, K., O'SULLIVAN, P. B., and FOSTER, D. A. 2002. Shaping the Australian crust over the last 300 million years: insights from fission track thermotectonic imaging and denudation studies of key terranes. Australian Journal of Earth Sciences **49**, 697-717. doi: 10.1046/j.1440-0952.2002.00942.x.

LI, Z. X., and POWELL, C. M. 2001. An outline of the palaeogeographic evolution of the Australasian region since the beginning of the Neoproterozoic. Earth-Science Reviews **53**, 237-277. doi: 10.1016/S0012-8252(00)00021-0.

LINC ENERGY LTD 2013. Independent reports confirm significant potential for Linc Energy's shale oil in the Arckaringa Basin. ASX Announcement 23/01/2013.

LUDBROOK, N. H. 1967. Permian deposits of South Australia and their fauna. Transactions of The Royal Society of South Australia **91**, 65-92. doi.

MACQUAKER, J. H. S., KELLER, M. A., and DAVIES, S. J. 2010. Algal Blooms and "Marine Snow": Mechanisms That Enhance Preservation of Organic Carbon in Ancient Fine-Grained Sediments. Journal of Sedimentary Research **80**, 934-942. doi: 10.2110/jsr.2010.085.

MACQUAKER, J. H. S., TAYLOR, K. G., and GAWTHORPE, R. L. 2007. High-Resolution Facies Analyses of Mudstones: Implications for Paleoenvironmental and Sequence Stratigraphic Interpretations of Offshore Ancient Mud-Dominated Successions. Journal of Sedimentary Research **77**, 324-339. doi: 10.2110/jsr.2007.029.

MACQUAKER, J. H. S., TAYLOR, K. G., KELLER, M., and POLYA, D. 2014. Compositional controls on early diagenetic pathways in fine-grained sedimentary rocks: Implications for predicting unconventional reservoir attributes of mudstones. AAPG Bulletin **98**, 587–603. doi.

MARUOKA, T., KOEBERL, C., HANCOX, P. J., and REIMOLD, W. U. 2003. Sulfur geochemistry across a terrestrial Permian–Triassic boundary section in the Karoo Basin, South Africa. Earth and Planetary Science Letters **206**, 101-117. doi: 10.1016/S0012-821X(02)01087-7.

MENPES, S. A. 2012. Unconventional hydrocarbon potential of the Arckaringa Basin, South Australia. In Ambrose, G. J., and Scott, J. ed.^eds. In Central Australian Basins Symposium III. Petroleum Exploration Society of Australia, Special Publication, 1-7.

MENPES, S. A. 2013. Organic Rich Shale in Permian Fjords – A Potential Resource Play in the Arckaringa Basin, South Australia. In ed.^eds. In AAPG Annual Convention and Exhibition. Search and Discovery Article #10538

MENPES, S. A., KORSCH, R. J., and CARR, L. K. 2010a 2008 Gawler Craton-Officer Basin-Musgrave Province-Amadeus Basin (GOMA) seismic survey, 08GA-OM1: Geological interpretation of the Arckaringa Basin (Presentation). In J., K. R., and N., K. ed.^eds. GOMA (Gawler Craton-Officer Basin-Musgrave Province-Amadeus Basin) Seismic and MT Workshop 2010. . ed. Geoscience Australia, Record 2010/39, pp. 16-31.

MENPES, S. A., KORSCH, R. J., and CARR, L. K. 2010b 2008 Gawler Craton-Officer Basin-Musgrave Province-Amadeus Basin (GOMA) seismic survey, 08GA-OM1: Geological interpretation of the Arckaringa Basin. In J., K. R., and N., K. ed.^eds. GOMA (Gawler Craton-Officer Basin-Musgrave Province-Amadeus Basin) Seismic and MT Workshop 2010. . ed. Geoscience Australia, Record 2010/39, pp. 16-31.

MEYER, K. M., and KUMP, L. R. 2008. Oceanic Euxinia in Earth History: Causes and Consequences. Annual Review of Earth and Planetary Science **36**, 251-288. doi: 10.1146/annurev.earth.36.031207.124256.

MOORE, P. S. 1982. Hydrocarbon potential of the Arckaringa Region, central South Australia. Australian Petroleum Exploration Association **21**, 237-253. doi.

MURRAY, J. W., STEWART, K., KASSAKIAN, S., KRYNYTZKY, M., and DIJULIO, D. 2007 Oxic, suboxic, and anoxic conditions in the Black Sea. In Yanko-Hombach, V., Gilbert, A., Panin, N., and Dolukhanov, P. M. ed.^eds. The Black Sea Flood Question: Changes in Coastline, Climate, and Human Settlement. ed. Kluwer, Dordrecth, Netherlands, pp.

NEUMANN, N. L., SKIRROW, R. G., FRASER, G. L., KORSCH, R. J., PREISS, W. V., COWLEY, W. M., and BLEWETT, R. S. 2010 Implications for regional energy and mineral systems of the 08GA-OM1 (GOMA) deep seismic reflection survey in the northern Gawler Craton to Amadeus Basin, South Australia and the Northern Territory In J., K. R., and N., K. ed.^eds. GOMA (Gawler Craton-Officer Basin-Musgrave Province-Amadeus Basin) Seismic and MT Workshop 2010. . ed. Geoscience Australia, Record 2010/39, pp. 152-162.

PEIZHEN, Z., MOLNAR, P., and DOWNS, W. R. 2001. Increased sedimentation rates and grain sizes 2–4 Myr ago due to the infuence of climate change on erosion rates. Nature **410**, 891-897. doi.

PETERS, K. E., and MOLDOWAN, J. M. 1993. The biomarker guide: Interpreting molecular fossils in petroleum and ancient sediments. ed.

PHILP, R. P., and GILBERT, T. D. 1986. Biomarker distributions in Australian oils predominantly derived from terrigenous source material. Organic Geochemistry **10**, 73-84. doi: 10.1016/0146-6380(86)90010-0.

PIASECKI, S., and STEMMERIK, L. 1991. Late Permian anoxia in central East Greenland. Geological Society Special Publication **58**, 275-290. doi: 10.1144/GSL.SP.1991.058.01.18.

POPPE, L. J., PASKEVICH, V. F., HATHAWAY, J. C., and BLACKWOOD, D. S. 2001. A Laboratory Manual for X-ray Powder Diffraction. Open-File Report 01-041.

PRESTON, J. C., and EDWARDS, D. S. 2000. The petroleum geochemistry of oils and source rocks from the northern Bonaparte Basin, offshore northern Australia. APPEA **40**, 257-282. doi.

PRICE, P. L., FILATOFF, J., WILLIAMS, A. J., PICKERING, S. A., and WOOD, G. R. 1985. Late Palaeozoic and Mesozoic palynostratigraphical units. Report 274/25. CSR Oil and Gas Division. (unpubl.).

REZAEE, M. R., and SCHULZ-ROJAHN, J. 1998. Application of Quantitative Back‐Scattered Electron Image Analysis in Isotope Interpretation of Siderite Cement: Tirrawarra Sandstone, Cooper Basin, Australia. International Association of Sedimentologists, Special Publications **26**, 461-481. doi.

SAELEN, G., RAISWELL, R., TALBOT, M. R., SKEI, J. M., and BOTTRELL, S. H. 1993. Heavy sedimentary sulfur isotopes as indicators of super-anoxic bottom-water conditions. Geology **21**, 1091-1094. doi.

SCHIEBER, J. 1999. Microbial mats in terrigenous clastics; the challenge of identification in the rock record. PALAIOS **14**, 3-12. doi: 10.2307/3515357.

SCHIEBER, J., SOUTHARD, J. B., and SCHIMMELMANN, A. 2010. Lenticular Shale Fabrics Resulting from Intermittent Erosion of Water-Rich Muds—Interpreting the Rock Record in the Light of Recent Flume Experiments. Journal of Sedimentary Research **80**, 119-128. doi: 10.2110/jsr.2010.005.

SHERROD, L., DUNN, G., PETERSON, G., and KOLBERG, R. 2002. Inorganic carbon analysis by modified pressure-calcimeter method. Soil Science Society of America Journal **66**, 299-305. doi.

SINNINGHE DAMSTE, J. S., and DE LEEUW, J. W. 1990. Analysis, structure and geochemical significance of organically-bound sulphur in the geosphere: State of the art and future research. Organic Geochemistry **16**, 1077-1101. doi: 10.1016/0146-6380(90)90145-P.

SINNINGHE DAMSTÉ, J. S., RIJPSTRA, W. I. C., COOLEN, M. J. L., SCHOUTEN, S., and VOLKMAN, J. K. 2007. Rapid sulfurisation of highly branched isoprenoid (HBI) alkenes in sulfidic Holocene sediments from Ellis Fjord, Antarctica. Organic Geochemistry **38**, 128-139. doi: 10.1016/j.orggeochem.2006.08.003.

SPECZIK, S. 1995. The Kupferschiefer mineralization of Central Europe: New aspects and major areas of future research. Ore Geology Reviews **9**, 411-426. doi: 10.1016/0169-1368(94)00022-G.

STICKLEY, C. E., PIKE, J., LEVENTER, A., DUNBAR, R., DOMACK, E. W., BRACHFELD, S., MANLEY, P., and MCCLENNAN, C. 2005. Deglacial ocean and climate seasonality in laminated diatom sediments, Mac.Robertson Shelf, Antarctica. Palaeogeography, Palaeoclimatology, Palaeoecology **227**, 290-310. doi: 10.1016/j.palaeo.2005.05.021.

SUÁREZ-RUIZ, I., FLORES, D., FILHO, J. G. M., and HACKLEY, P. C. 2012. Review and update of the applications of organic petrology: Part 1, geological applications. International Journal of Coal Geology **99**, 54-112. doi: 10.1016/j.coal.2012.02.004.

SYVITSKI, J. P. M., ANDREWS, J. T., and DOWDESWELL, J. A. 1996. Sediment deposition in an iceberg-dominated glacimarine environment, East Greenland: basin fill implications. Global and Planetary Change **12**, 251-270. doi: 10.1016/0921-8181(95)00023-2.

TAYLOR, G. H., TEICHMÜLLER, M., DAVIS, A., DIESSEL, C. F. K., LITTKE, R., and ROBERT, P. 1998. Organic Petrology. ed. Gebrüder Borntraeger, Berlin.

TEGELAAR, E. W., DE LEEUW, J. W., DERENNE, S., and LARGEAU, C. 1989. A reappraisal of kerogen formation. Geochimica et Cosmochimica Acta **53**, 3103-3106. doi: 10.1016/0016-7037(89)90191-9.

TEN HAVEN, H. L., DE LEEUW, J. W., PEAKMAN, T. M., and MAXWELL, J. R. 1986. Anomalies in steroid and hopanoid maturity indices. Geochimica et Cosmochimica Acta **50**, 853-855. doi: 10.1016/0016-7037(86)90361-3.

TOWNSEND, I. J., and LUDBROOK, N. H. 1975. Revision of Permian and Devonian nomenclature of four formations in and below the Arckaringa Basin. South Australia Geological Survey, Quarterley Geological Notes **54**, 2-7. doi.

VEEVERS, J. J. 2006. Updated Gondwana (Permian–Cretaceous) earth history of Australia. Gondwana Research **9**, 231-260. doi: 10.1016/j.gr.2005.11.005.

WAKEHAM, S. G., SINNINGHE DAMSTÉ, J. S., KOHNEN, M. E. L., and DE LEEUW, J. W. 1995. Organic sulfur compounds formed during early diagenesis in Black Sea sediments. Geochimica et Cosmochimica Acta **59**, 521-533. doi: 10.1016/0016-7037(94)00361-O.

WEISHEIT, A., BONS, P. D., DANIŠÍK, M., and ELBURG, M. A. 2014. Crustal-scale folding: Palaeozoic deformation of the Mt Painter Inlier, South Australia. Geological Society, London, Special Publications **394**, 53-77. doi: 10.1144/sp394.9.

WEISSERT, H., and MOHR, H. 1996. Late Jurassic climate and its impact on carbon cycling. Palaeogeography, Palaeoclimatology, Palaeoecology **122**, 27-43. doi.

WOHLING, D., KEPPEL, M., FULTON, S., COSTAR, A., SAMPSON, L., and BERENS, V. 2013. Australian Government Initiative on Coal Seam Gas and Large Coal Mining: Arckaringa Basin and Pedirka Basin Groundwater Assessment Projects. DEWNR Technical Report 2013/11. Government of South Australia, through Department of Environment, Water and Natural Resources. Adelaide.

WOPFNER, H. 1970. Permian paleogeography and depositional environment of the Arckaringa Basin, South Australia. In ed.^eds. In Proceedings and Papers IUGS Sub-Commission on Gondwana stratigraphy and palaeontology. Second Gondwana symposium. Council for Scientific and Industrial Research, Scientia, South Africa, 273-291.

WOPFNER, H. 1980 Development of Permian intracratonic basins in Australia. In Cresswell, M. M., and Vella, P. ed.^eds. 5th International Gondwana Symposium, Wellington, New Zealand, 1980. ed., pp. 185-190.

APPENDIX A: ORGANIC GEOCHEMISTRY DATA

Table A1: Summary of samples used for organic geochemistry.

Sample	Depth sampled (m)	TOC	Facies	Interval
2053195*	960.24	0.11	Bioturbated Facies	Organic lean
960 (x1)[CI]	960.005 – 960.05	1.33	Mass Flow Facies	Organic lean
960 (x2)*	960.005 – 960.05	1.33	Mass Flow Facies	Organic lean
960[CO]	960.005 – 960.05	1.33	Mass Flow Facies	Organic lean
960 varve*	959.96 – 959.945, 959.995 – 960.005	5.51	Pelagic Facies 2a	Organic rich
962.54*	962.54 – 962.518, 962.412 – 962.10	5.51[E]	Pelagic Facies 2a	Organic rich
2053188*	966.35	8.18	Pelagic Facies 2b	Organic rich
2053188[CO]	966.35	8.18	Pelagic Facies 2b	Organic rich

"960" samples were sub-sampled from 2071886. Sample "962.54" was sub-sampled from 2071882.
* samples used for comparative analyses
[CO] Contaminated core outer surface sample
[CI] Laboratory contaminated inner sample
[E] Extrapolated TOC based on '960 varve' average TOC

APPENDIX B: XRD DATA

Table B1: Clay mineral fraction present within a selection of Arck 1 core samples based on randomly-orientated powdered and orientated air dried and ethylene glycol X-ray diffraction (XRD) results. Total organic carbon (TOC) values have been included to facilitate analysis. 'X' represents mineral presence and '?' indicates that a mineral phase may be present, though with uncertainty.

Sample	Illite	Smectite	Mixed I-S	Kaolinite	Chlorite	TOC
2053194	X	X	X	X	X	3.04
2053196	X	?	X	X	X	7.74
2053198	X	X	X	X	X	4.64

Table B2: Mineral phases present within a selection of Arck 1 core samples, based on bulk powder mineralogy X-ray diffraction (XRD) results. The shaded boxes marked with an 'X' represent mineral presence. The '?' indicates that a mineral phase may be present, though with uncertainty

Sample (2053....)	Quartz	Albite	Illite /mica	K-feldspar	Kaolinite	Leucite (?)	Mixed I-S	Chlorite	Siderite	Dolomite	Magnesite	Kutnohorite	Calcite	Jarosite	Gypsum	Apatite	Pyrite	TOC
165	X	X	X	X	X		X	X	X						X		X	1.01
180	X	X	X	X	X			X		X	?	X		X	X	?	X	3.70
183	X	X	X	X	X			X				X		X	X	?	X	4.38
188	X	X	X	X	X			X						X	X		X	8.18
190	X	X	X		X	X	X							X	X		X	0.56
191	X	X	X		X	X	X	X						X	X		X	8.24
192	X	X	X		X		?	X						X	X		X	1.81
193	X	X	X		X	X	X	X						X	X		X	3.65
194	X	X	X	X	X		X	X						X	X		X	3.04
195	X		X		X					X	X	X	?			X	X	0.11
196	X	X	X		X	X	X	X						X	X		X	7.74
197	X	X	X		X			X		X		X		X	X	X	X	4.78
198	X	X	X	X	X	X	?	X						X	X		X	4.64
307A	X	X	X		X	X	?	X				X		X	X	X	X	4.60
307B	X	X	X	X	X		?	X		X			X	X	X	X	X	1.76
311	X		X	?	X			X	X	X	X	X	X					0.23
315	X	X	X	X	X		X	X	?	?	?			X	X		X	7.59
327	X		X	?	X	X		X	X	X	?	X	X	X		?	X	0.88
332	X	X	X		X	X	?	X	X	X	X	X	X	X	X	X	X	1.29
336	X	X	X	X	X	X	X	X	?	X	X		?	X	X		X	5.60
339	X		X	?	X	X	X	?						X	X	?	X	2.11
362	X	X	X	X	X	X	?	X	?					X	X		X	3.36
363	X	X	X		X		X	X	?	X	?	X		X	?	X	X	8.33
379	X	X	X	X	X	X	X	X	?		X			X	X		X	9.71
383	X	X	X		X	X	X	X	X	?	X		?	?	?	X	X	2.81

APPENDIX C: SAMPLE DATA

Table C1: Supporting data for Arck 1 core sub-samples and analyses performed on each, exculding organic geochemistry analyses (Appendix A, Table A1). Formations: B = Boorthanna; SR = Stuart Range; MT = Mount Toondina. Analyses: SRA = Source Rock Analyser; TH-GC-MS = thermal extraction GC-MS (gas chromatography-mass spectrometry); MSSV-GC-MS = micro-scaled sealed vessel pyrolysis GC-MS; XRD = X-Ray Diffraction; SEM = Scanning Electron Microscope.

Sample	Depth (m)	To Depth (m)	Formation	TOC (%)	Analysis							
					SRA	TH-GC-MS	MSSV-GC-MS	XRD (Bulk)	XRD (Clay)	Thin Section	Organic Petrog.	SEM
2053149	994.10		B	0.07								
2053150	993.36		B	-0.07						**X**		
2053151	990.17		B	0.08								
2053152	989.70		B	0.03								
2053153	986.40		B	0.02								
2053154	985.12		B	0.01								
2053155	985.08		B	0.04								
2053156	983.92		B	0.01								
2053157	983.32		B	0.17								
2053158	982.27		B	-0.04								
2053159	982.09		B	-0.36								
2053160	980.49		B	0.22								
2053161	980.06		B	0.45								
2053162	979.89		B	-0.10								
2053163	979.10		B	0.13								
2053164	978.05		B	0.51								
2053165	976.15		B	1.01	**X**						**X**	**X**
2053166	975.88		B	1.49								
2053167	975.60		B	1.93								
2053168	975.39		B	1.52	**X**							
2053169	975.21		B	1.60	**X**							
2053170	975.11		B	1.96								
2053171	974.84		B	1.35								
2053172	974.64		B	0.82								
2053173	973.96		B	0.86								

2053174	973.17		B	4.16	**X**					**X**		
Sample	**Depth (m)**	**To Depth (m)**	**Formation**	**TOC (%)**	**Analysis**							
					SRA	TH-GC-MS	MSSV-GC-MS	XRD (Bulk)	XRD (Clay)	Thin Section	Organic Petrog.	SEM
2053175	972.82		B	2.19								
2053176	972.67		B	1.69	**X**							
2053177	972.56		B	0.36								
2053178	972.44		B	1.56								
2053179	972.24		B	1.87						**X**		
2053180	971.59		B	3.70	**X**			**X**		**X**		
2053181	970.14		B	0.94	**X**							
2053182	970.03		B	4.19								
2053183	969.98		SR	4.38	**X**			**X**				
2053184	969.38		SR	2.08	**X**							
2053185	969.02		SR	6.81	**X**							
2053186	968.96		SR	3.48	**X**							
2053187	968.70		SR	6.46	**X**	**X**	**X**					
2053188	966.35		SR	8.18	**X**	**X**		**X**			**X**	**X**
2053189	966.22		SR	4.19	**X**							
2053190	966.14		SR	0.56	**X**			**X**				
2053191	965.10		SR	8.24	**X**	**X**		**X**			**X**	**X**
2053192	964.71		SR	1.81	**X**			**X**				
2053193	963.04		SR	3.65	**X**			**X**				
2053194	960.82		SR	3.04	**X**			**X**	**X**		**X**	**X**
2053195	960.24		SR	0.11	**X**			**X**				
2053196	959.97		SR	7.74	**X**			**X**	**X**	**X**	**X**	**X**
2053197	957.60		SR	4.78	**X**			**X**			**X**	**X**
2053198	955.79		SR	4.64	**X**			**X**	**X**		**X**	**X**
2053307A	952.59		SR	4.60	**X**			**X**			**X**	**X**
2053307B	952.59		SR	1.76	**X**			**X**				
2053308	951.30		SR	4.91	**X**							
2053309	951.25		SR	4.57	**X**							
2053310	951.03		SR	2.90	**X**							
2053311	949.87		SR	0.23	**X**			**X**				
2053312	949.65		SR	1.56	**X**							
2053313	947.56		SR	4.46	**X**							

2053314	946.34		SR	4.05	**X**							
Sample	**Depth (m)**	**To Depth (m)**	**Formation**	**TOC (%)**	**Analysis**							
					SRA	TH-GC-MS	MSSV-GC-MS	XRD (Bulk)	XRD (Clay)	Thin Section	Organic Petrog.	SEM
2053315	945.12		SR	7.59	**X**			**X**				
2053316	944.90		SR	5.46	**X**							
2053317	943.77		SR	5.93	**X**							
2053318	943.05		SR	6.80	**X**							
2053319	942.34		SR	5.78	**X**							
2053320	941.00		SR	-0.11	**X**							
2053321	940.80		SR	5.91								
2053322	940.00		SR	4.66								
2053323	938.75		SR	6.90	**X**							
2053324	937.52		SR	6.53								
2053325	937.15		SR	4.57								
2053326	934.76		SR	3.44								
2053327	934.59		SR	0.88	**X**			**X**		**X**		
2053328	934.00		SR	6.49								
2053329	932.40		SR	6.52	**X**							
2053330	931.10		SR	5.13								
2053331	930.65		SR	4.30	**X**							
2053332	928.94		SR	1.29	**X**			**X**		**X**	**X**	**X**
2053333	927.00		SR	1.14								
2053334	926.44		SR	5.87	**X**	**X**	**X**					
2053335	926.00		SR	3.28	**X**	**X**						
2053336	924.80		SR	5.60	**X**			**X**				
2053337	924.42		SR	4.55								
2053338	924.27		SR	4.04								
2053339	923.03		SR	2.11	**X**			**X**			**X**	**X**
2053340	921.81		SR	4.71								
2053341	919.60		SR	4.87	**X**							
2053342	918.84		SR	3.43								
2053343	918.06		SR	6.36								
2053344	917.49		SR	3.41	**X**							
2053345	917.02		SR	4.21	**X**	**X**						
2053346	916.27		SR	7.95	**X**							

2053347	916.05		SR	8.69	X							
Sample	**Depth (m)**	**To Depth (m)**	**Formation**	**TOC (%)**	**Analysis**							
					SRA	TH-GC-MS	MSSV-GC-MS	XRD (Bulk)	XRD (Clay)	Thin Section	Organic Petrog.	SEM
2053348	915.48		SR	4.20						X		
2053349	915.36		SR	6.20								
2053350	914.66		SR	3.57								
2053351	914.56		SR	3.53								
2053352	914.32		SR	4.69								
2053353	914.03		SR	2.07	X							
2053354	913.82		SR	3.88								
2053355	913.50		SR	3.83								
2053356	912.92		SR	5.30								
2053357	912.24		SR	5.72								
2053358	911.72		SR	5.04								
2053359	911.37		SR	7.81	X							
2053360	910.37		SR	5.53								
2053361	910.00		SR	4.05								
2053362	909.18		SR	3.36	X			X				
2053363	908.00		SR	8.33	X			X				
2053364	907.53		SR	7.01								
2053365	906.33		SR	7.90	X							
2053366	906.17		SR	4.89	X							
2053367	905.63		SR	4.23	X	X	X					
2053368	905.50		SR	4.44								
2053369	904.78		SR	4.21								
2053370	904.72		SR	3.92								
2053371	904.47		SR	2.63	X							
2053372	904.27		SR	4.90								
2053373	903.72		SR	5.84								
2053374	903.08		SR	4.38								
2053375	901.98		SR	5.20	X							
2053376	901.70	901.63	SR	4.15								
2053377	900.73	900.76	SR	7.52	X							
2053378	899.25		SR	6.09								
2053379	898.00		SR	9.71	X			X			X	X

2053380	897.84	897.81	SR	6.88								
Sample	**Depth (m)**	**To Depth (m)**	**Formation**	**TOC (%)**	**Analysis**							
					SRA	TH-GC-MS	MSSV-GC-MS	XRD (Bulk)	XRD (Clay)	Thin Section	Organic Petrog.	SEM
2053381	897.26	897.31	SR	6.11	**X**							
2053382	896.06	896.14	SR	2.22						**X**		
2053383	896.00		SR	2.81	**X**			**X**		**X**		
2053384	895.29	895.24	MT	0.93	**X**					**X**		
2053385	894.44	894.53	MT	1.69						**X**		
2053386	894.04		MT	1.85								
2053387	893.76		MT	2.74	**X**							
2053388	893.42		MT	1.93						**X**		
2053389	892.72	892.76	MT	2.25								
2053390	892.42		MT	2.39								
2053391	892.01	891.94	MT	1.73								
2053392	891.02	890.96	MT	1.04								
2053393	890.46	890.41	MT	0.98								
2053394	890.14	890.09	MT	1.39								
2053395	889.72	889.63	MT	0.94								
2053396	889.35	889.28	MT	0.64								
2053397	889.02	888.96	MT	0.28								
2053398	888.81	888.73	MT	0.89								
2053399	888.50	888.43	MT	1.40	**X**							
2053400	887.05	886.99	MT	1.25								
2053401	886.55	886.50	MT	4.72	**X**							
2053402	885.90	885.85	MT	2.65								
2053403	885.05	885.00	MT	4.10								
2053404	882.37	882.30	MT	3.39								
2053405	877.06	877.02	MT	0.15								
2053406	876.80	876.74	MT	2.26								
2053407	876.64	876.60	MT	2.45								
2053408	876.13	876.06	MT	2.29	**X**							
2071876	970.45		SR	5.46								
2071877	968.50		SR	2.44								
2071878	968.00		SR	8.10								
2071879	967.00		SR	10.19								

2071880	964.00		SR	8.75								
Sample	**Depth (m)**	**To Depth (m)**	**Formation**	**TOC (%)**	**Analysis**							
					SRA	TH-GC-MS	MSSV-GC-MS	XRD (Bulk)	XRD (Clay)	Thin Section	Organic Petrog.	SEM
2071881	963.50		SR	8.47								
2071882	962.50		SR	4.32								
2071883	962.00		SR	9.66								
2071884	961.40		SR	4.36								
2071886	959.50		SR	6.48								
2071887	959.00		SR	8.52								
2071888	958.00		SR	6.49								
2071889	957.25		SR	6.34								
2071890	956.75		SR	6.75								
2071891	954.00		SR	8.17								
2071892	953.50		SR	5.86								
2071893	953.00		SR	4.30								
2071894	952.25		SR	4.24								
2071895	951.75		SR	5.89								
2071896	950.70		SR	6.65								
2071897	950.55		SR	4.07								
2071898	950.40		SR	3.96								
2071899	950.25		SR	6.22								
2071900	950.10		SR	2.86								
2071901	949.95		SR	6.72								
2071902	949.90		SR	0.99								
A	969.16		SR	1.28								
B	968.06		SR	1.33								
C	963.31		SR	1.36								
D	962.96		SR	1.29							**X**	**X**
E	961.56		SR	1.71								
F	960.03		SR	1.56								
G	960.03		SR	1.40								
H	959.03		SR	3.79								
I	957.86		SR	5.55							**X**	**X**
J	956.06		SR	3.21								
K	955.9		SR	6.16								

L	951.56		SR	6.01								

Table C2: Supporting data for Cootanoorina 1 core and cutting subsamples and analyses performed on each. Formations: C = Cootanoorina; B = Boorthanna; SR = Stuart Range; MT = Mount Toondina.

Sample	Depth (m)	To Depth (m)	Formation	Core/Cutting	TOC (%)	Analysis
						SRA
2066664	948.06		C	Core	1.79	**X**
2066665	947.80		C	Core	1.50	**X**
2066666	947.34		C	Core	1.70	**X**
2066667	946.48		C	Core	2.16	**X**
2066668	945.88		C	Core	0.79	**X**
2066669	945.20		C	Core	1.73	**X**
2066670	944.45		C	Core	1.51	**X**
2066671	944.92		C	Core	1.51	**X**
2066672	944.15		C	Core	2.16	**X**
2066673	943.60		C	Core	1.97	**X**
2066674	943.00		C	Core	1.04	**X**
2066675	928.42		C	Core	1.33	**X**
2066676	927.69		C	Core	0.52	**X**
2066677	926.69		C	Core	1.22	**X**
2066678	926.23		C	Core	0.72	**X**
2066679	925.37		C	Core	0.09	
2066680	888.86		B	Core	0.07	
2066681	888.23		B	Core	0.03	
2066682	873.65		B	Core	0.14	
2066683	872.83		B	Core	0.13	
2066684	718.96		SR	Core	0.10	
2066685	533.90		SR	Core	2.18	**X**
2066686	532.25		SR	Core	2.37	**X**
2066687	530.96		SR	Core	2.58	**X**
2066688	380.09		MT	Core	0.06	
2066691	868.68	871.73	B	Cutting	0.61	
2066692	865.63	868.68	B	Cutting	0.60	
2066693	862.58	865.63	B	Cutting	0.70	
2066694	859.54	862.58	B	Cutting	0.83	
2066695	856.49	859.54	B	Cutting	0.87	
2066696	853.44	856.49	B	Cutting	0.85	
2066697	850.39	853.44	B	Cutting	0.80	
2066698	847.34	850.39	B	Cutting	0.83	
2066699	844.30	847.34	B	Cutting	0.63	
2066700	841.25	844.30	B	Cutting	0.77	
2066701	838.20	841.25	B	Cutting	0.84	
2066702	835.15	838.20	B	Cutting	0.95	
2066703	832.10	835.15	B	Cutting	0.80	
2066704	829.06	832.10	B	Cutting	0.77	
2066705	826.01	829.06	B	Cutting	0.77	
2066706	822.96	826.01	B	Cutting	0.92	
2066707	819.91	822.96	B	Cutting	0.86	
2066708	816.86	819.91	B	Cutting	1.32	
2066709	813.82	816.86	B	Cutting	1.11	
2066710	810.77	813.82	B	Cutting	0.81	
2066711	807.72	810.77	B	Cutting	0.50	
2066712	804.67	807.72	B	Cutting	0.83	
2066713	801.62	804.67	B	Cutting	0.48	
2066714	798.58	801.62	B	Cutting	0.76	
2066715	795.53	798.58	B	Cutting	1.59	
2066716	792.48	795.53	B	Cutting	0.54	

Sample	Depth (m)	To Depth (m)	Formation	Core/Cutting	TOC (%)	Analysis
						SRA
2066717	789.43	792.48	B	Cutting	0.70	
2066718	786.38	789.43	B	Cutting	0.86	
2066719	783.34	786.38	B	Cutting	0.68	
2066720	780.29	783.34	B	Cutting	0.65	
2066721	777.24	780.29	B	Cutting	0.66	
2066722	774.19	777.24	SR	Cutting	0.68	
2066723	771.14	774.19	SR	Cutting	0.87	
2066724	768.10	771.14	SR	Cutting	0.75	
2066725	765.05	768.10	SR	Cutting	0.80	
2066726	762.00	765.05	SR	Cutting	0.76	
2066727	758.95	762.00	SR	Cutting	0.70	
2066728	755.90	758.95	SR	Cutting	0.73	
2066729	752.86	755.90	SR	Cutting	0.98	
2066730	749.81	752.86	SR	Cutting	0.80	
2066731	746.76	749.81	SR	Cutting	0.71	
2066732	743.71	746.76	SR	Cutting	0.87	
2066733	740.66	743.71	SR	Cutting	0.79	
2066734	737.62	740.66	SR	Cutting	0.92	
2066736	731.52	734.57	SR	Cutting	0.96	
2066737	728.47	731.52	SR	Cutting	-0.49	
2066738	725.42	728.47	SR	Cutting	1.14	
2066739	722.38	725.42	SR	Cutting	1.91	
2066740	719.33	722.38	SR	Cutting	1.48	
2066741	716.28	719.33	SR	Cutting	1.82	
2066742	713.23	716.28	SR	Cutting	2.71	
2066743	710.18	713.23	SR	Cutting	2.87	
2066744	707.14	710.18	SR	Cutting	3.44	
2066745	704.09	707.14	SR	Cutting	3.23	
2066746	701.04	704.09	SR	Cutting	3.66	

Table C3: Supporting data for Lambina 1 core and cutting subsamples and analyses performed on each. Formations: B = Boorthanna; MT = Mount Toondina.

Sample	Depth (m)	To Depth (m)	Formation	Core/Cutting	TOC (%)	Analysis
						SRA
2131267	377.95	381.00	MT	Cutting	0.26	**X**
2131268	411.48	414.53	MT	Cutting	0.30	**X**
2131269	435.86	438.91	B	Cutting	0.55	**X**
2131270	440.13	441.96	B	Core	0.29	**X**
2131271	441.96	444.09	B	Core	N/A	